Baltimore Flash Flood Forecasting Project: Final Report

James A. Smith

Mary Lynn Baeck

Julie R. Javier

Katherine L. Meierdiercks

Department of Civil and Environmental Engineering

Princeton University

Princeton, New Jersey

January 4, 2006

Summary and Conclusions

The utility of distributed hydrologic models and high-resolution WSR-88D radar rainfall estimates for flash flood forecasting in urban drainage basins is examined through analyses carried out for the Baltimore Flash Flood Forecasting Project (BFFP). The Network Model, which is a computationally efficient distributed hydrologic model, was implemented for the Dead Run and Moores Run watersheds in the Baltimore metropolitan region. The model consists of a simple infiltration model (Green-Ampt with moisture redistribution) and a GIUH-based representation of hillslope and channel response. The model was run in real time during the summers of 2004 and 2005 with a feed of Digital Hybrid Reflectivity (DHR) data from the Sterling, Virginia WSR-88D. Analyses in this report focus on the 14.3 km^2 Dead Run watershed in Baltimore County, Maryland and are based on a nested network of 6 stream gages and a network of 18 rain gage stations in the Dead Run watershed. Analyses are also presented for flash flood events in the Philadelphia metropolitan region to reinforce the conclusions drawn from the Baltimore study sites. Principal conclusions of this study are the following:

1. Distributed hydrologic models and high-resolution WSR-88D rainfall rate fields can provide important elements of site-specific flash flood forecasting systems in small urban watersheds. The hydrologic response of Dead Run at the 14.3 km^2 scale can be accurately modeled using the Network Model and bias-corrected WSR-88D rainfall fields. The GIUH-based framework of the Network Model provides a computationally

efficient modeling framework for flash flood forecasting.

2. A major limitation on the accuracy of flash flood forecasting in urban watersheds is imposed by stormwater management infrastructure. Heterogeneity of flood response in the Dead Run watershed is closely linked with stormwater management infrastructure.

3. Hydraulic controls imposed by valley bottom constrictions associated with bridges and bridge abutments are a dominant element of the extreme flood response of small urban watersheds. For the three largest flood peaks in Dead Run, including the flood of record on 7 July 2004 which had a peak "unit discharge" (discharge divided by drainage area) of approximately 18 $m^3\ s^{-1}\ km^{-2}$, hydrologic model forecasts do not capture the pronounced attenuation of flood peaks. As a consequence, hydrologic model forecasts of flood peak magnitude and the timing of flood peaks will exhibit errors that are strongly dependent on flood magnitude.

4. There is potential for improving model forecasts of flash floods in urban drainage basins through the utilization of information on initial soil moisture storage. A simple first step would be to incorporate a seasonally varying initial moisture content.

5. Errors in the rainfall field are the largest sources of uncertainty in quantitative flash flood forecasting. Bias correction of radar rainfall estimates with rain gage observations is an important element of flash flood forecasting systems. The multiplicative bias is a dominant source of error in WSR-88D radar rainfall estimates for

flash-flood producing storms. Bias in radar rainfall estimates for the Dead Run basin exhibits a systematic seasonal variation that is tied to the convective potential of the storm environment. Bias also exhibits dependence on flood magnitude, with a systematic underestimation of rainfall for the most extreme floods (using the convective Z-R relationship). Similar features are observed for the four flash flood events in the Philadelphia metropolitan region. The multiplicative bias for rainfall estimates from the KDIX WSR-88D for the four flood events varied around 1.4 for the convective Z-R relationship (and 0.7 for the tropical Z-R relationship). Analyses suggest that probabilistic quantitative precipitation estimation (PQPE) procedures should exploit the magnitude-dependent error structure of radar rainfall estimates. Analyses also suggest that "local" bias correction using dense urban rain gage networks could significantly enhance flash flood forecasts in high-risk areas.

6. There is large spatial variability in flash-flood producing rainfall over the 14.3 km^2 Dead Run drainage basin. The capability of WSR-88D radar rainfall estimates to resolve spatial variation of storm total rainfall varies markedly from storm to storm. For 22 of 35 storm events during the 2003-2005 observing period, the correlation between storm total rainfall from rain gages and radar was greater than 0.5. For several major flood events, the correlation was less than 0 (see item 8 below).

7. Bias-corrected, basin-averaged rainfall rate estimates at 60 minute time interval are directly related to peak discharge for Dead Run at 14.3 km^2 scale. Averaging over longer and shorter time periods reduces information content concerning peak

discharge. The predictability of flood peak magnitudes decreases as the basin scale decreases below 10 km^2 due in large part to the increasing errors in radar rainfall estimates at shorter time scales and smaller spatial scales. The flood response time in Dead Run decreases from 60 minutes at 14.3 km^2 scale to approximately 15 minutes at 1.6 km^2 scale, yet peak discharge in the DR2 watershed (which has drainage area of 1.6 km^2) is more closely linked to 60 minute basin-averaged rain rates than 15 minute basin-averaged rain rates.

8. For the 7 July 2004 storm, which produced the flood of record in Dead Run, WSR-88D rainfall estimates capture the extreme flood-producing rainfall over Dead Run, but do not accurately reflect the detailed spatial structure of rainfall over the 14.3 km^2 watershed. Based on drop-size distribution observations from a Joss-Waldvogel disdrometer, it is shown that errors in rainfall rate estimates are tied to anomalous variation in drop-size distributions. It is also shown that simple polarimetric algorithms can adequately address these microphysical controls of extreme rain rates.

9. The second largest flood peak in Dead Run during the 2003 - 2005 observing period resulted from a storm that produced 75 - 100 mm of rain in the 1.2 km^2 DR1 subbasin during a period of less than 1 hour. WSR-88D rainfall estimates for Dead Run produce a maximum accumulation in the DR1 subbasin, but the bias-corrected rainfall estimates severely underestimate the maximum accumulations in DR1. Extreme rainfall rates were associated with a decaying thunderstorm system,

for which there was large vertical variation in reflectivity during the period of extreme rain rates over DR1. Rainfall analyses of the 28 June 2005 storm were also performed using 1-minute low level reflectivity fields from the BWI TDWR (Terminal Doppler Weather Radar) radar. Bias-corrected TDWR rainfall estimates not only capture the variation of rainfall over Dead Run, they also capture the 90-100 mm maximum in DR1. These analyses support prior conclusions that TDWR rainfall estimates hold substantial potential for improving flash flood forecasts in urban drainage basins.

10. The remnants of Tropical Storm Allison produced rainfall accumulations exceeding 200 mm in less than 12 hours on 16-17 June 2001 over an area of 100 km^2 in the headwaters of Little Neshaminy, Wissahickon and Pennypack Creeks in the Philadelphia metropolitan region. Flooding in Pennypack Creek resulted in 8 fatalities. The Network Model and WSR-88D rainfall estimates were used to simulate hydrologic response of Pennypack Creek at 20 km^2 (the location of the 8 fatalaties). Model analyses result in a peak discharge of 189.8 $m^3\ s^{-1}$ (unit discharge of 8.7 $m^3\ s^{-1}\ km^{-2}$) at 0226 UTC on 17 June 2001. The timing and magnitudes of the model response (there is no stream gage) are compared with observer reports and show good agreement. These analyses further illustrate the potential utility of site-specific flash flood forecasting models in ungaged, urban catchments.

1 Introduction

In this study, we examine the utility of distributed hydrologic models and high-resolution WSR-88D rainfall estimates for flash flood forecasting in small urban watersheds. The hydrologic model (Morrison and Smith, 2001; Giannoni et al., 2003; Zhang et al., 2003; Smith et al. 2005a, Hicks et al., 2005 and Slutzman and Smith, 2006) consists of a simple infiltration model and a GIUH-based representation of hill-slope and channel response. The structure of the hydrologic model is dictated by computational constraints on real-time flash-flood forecasting models. The forecasting model has been implemented for the 14.3 km^2 Dead Run watershed in Baltimore County, Maryland (see Smith et al,. 2005b and Nelson et al., 2005) and the 9.1 km^2 Moores Run watershed in Baltimore City (Smith et al. 2005a). During the summers of 2004 and 2005, the modeling system has run in real-time with a data feed of Digital Hybrid Reflectivity (DHR) fields from the Sterling, Virginia WSR-88D (Weather Surveillance Radar - 1988 Doppler) .

Extensive development of distributed hydrologic models for flood forecasting applications has occurred during the last decade (Burnash, 1995; Koren et al. 2004, Vieux, 2001; Vieux et al., 2004, Julien et al., 1995, Ogden et al., 2000; Butts et al., 2004; Carpenter and Georgakakos, 2004; Georgakakos et al., 2004; Ivanov et al., 2004; Reed et al., 2004; Vieux and Bedient, 2004; and Smith et al., 2004,). Similarly, there have been extensive efforts aimed at developing calibration procedures for hydrologic models (Duan et al., 1992; Gupta et al., 1998; Vrugt et al., 2005). In this study,

we assess the applicability of distributed hydrologic models for flash flood forecasting through model analyses in an urban watershed with a nested network of stream gaging stations. The focus of the study is on performance of flash flood forecasting systems for extreme floods.

Dead Run is a 14.3 km^2 tributary of the Gwynns Falls watershed in Baltimore County Maryland (Figs. 1 and 2). Gwynns Falls is the principal study watershed of the Baltimore Ecosystem Study (BES; see Groffman et al., 2003; and Smith et al. 2005b) and has a dense network of stream gages that have been deployed in connection with BES hydrologic monitoring activities. A nested network with 6 stream gages has been deployed in the Dead Run watershed at basin scales ranging from 1.2 to 14.3 km^2. The stream gaging network and a dense network of rain gages in Dead Run provide exceptional observational resources for assessment of flash flood forecasting systems in urban watersheds. In addition, the Dead Run watershed has experienced a number of major flood events in 2004 and 2005, including the flood of record in Dead Run, which occurred on 7 July 2004 (the stream gaging record for Dead Run extends back to the 1950s). The peak unit discharge for the 7 July 2004 flood at 14.3 km^2 scale was approximately 18 $m^3\ s^{-1}\ km^{-2}$. Floods on 27-28 July 2004 and 28 June 2005 had unit discharge peaks of approximately 4 $m^3\ s^{-1}\ km^{-2}$.

Radar rainfall estimation for flash flood forecasting in small, urban catchments is examined through analyses of radar and rain gage observations from the Dead Run drainage basin (Fig. 2; see Smith et al., 2005b and c; and Nelson et al., 2005).

Analyses are based on 36 storm events during the 2003 - 2005 period.

In this study, rainfall analyses are based largely on volume scan reflectivity observations from the Sterling, Virginia WSR-88D radar and storm total rainfall accumulations from a network of 18 double-gage platforms in the Dead Run watershed (Fig. 2). The Sterling WSR-88D radar is approximately 70 km from the Dead Run watershed. The rainfall distribution for flood-producing storms in urban environments can exhibit large variability in time and space (Odgen et al., 2000; Petersen et al., 1999; Changnon, 1999; Vieux and Bedient, 2004; Krajewski et al., 2003; Zhang et al., 2003; and Smith et al., 2002, 2005 a and b). A focus of this study is examining the capability to resolve the spatial and temporal distribution of rainfall from WSR-88D reflectivity observations for flash flood forecasting.

The report is organized as follows. In Section 2, we present a description of the Baltimore study watersheds used in this project. The Network Model is introduced in Section 3. Analyses of WSR-88D rainfall estimates for flash flood forecasting, based largely on intercomparisons with observations from the Dead Run rain gage network, are presented in Section 4. Network Model analyses of major flash floods are presented in Section 5. Analyses of flash flood events in the Philadelphia metropolitan region are presented in Section 6.

2 Study Watersheds

The Dead Run watershed was settled in the 18th century and has undergone intense urbanization since the late 1950s [Nelson et al., 2005]. The basin contains a diverse mix of urban and suburban development. As a tributary of the Gwynns Falls watershed, Dead Run has been extensively studied in connection with BES hydrologic investigations (see Smith et al. 2005b, Nelson et al. 2005). Hydrologic model analyses utilize observations collected during intensive summer field campaigns during the 2003 - 2005 time period.

A nested network of 5 stream gauges (denoted DR1 - DR5 in Fig. 2; see also Fig. 3) has been installed in the Dead Run watershed to augment the USGS stream gage at Franklintown (Fig. 2). Drainage area for the six stream gaging stations ranges from 1.2 to 14.3 km^2 (1.2 for DR1, 1.6 for DR2, 1.9 for DR5, 4.9 for DR3, 6.1 for DR4 and 14.3 km^2 for Franklintown). Time resolution of the discharge observations is 1 minute for the DR1 - DR5 stations and 5 minutes for Franklintown. Rating curves for the five new stream gauges (DR1 - DR5) have been developed from direct discharge measurements (Fig. 3) and hydraulic model studies (Smith et al., 2005b). Discharge data sets from these 6 stations play a central role in examining the performance of flash flood forecasting systems. Basin boundaries and stream channels were delineated from the USGS 1 arc second (30 m) Digital Elevation Model (DEM).

A network of 18 rain gauge stations has been deployed in the Dead Run watershed

(Fig. 2; see also Fig. 3). Each station has two Tru-check rain gauges (Fig. 3) which are separated by approximately 1 meter and read manually after each storm event (Smith et al., 2005b and c).

Polar reflectivity data from the Sterling WSR-88D are processed to rainfall rate fields at 5-minute and 1-km horizontal resolution for rainfall analyses [Baeck and Smith, 1998; Fulton et al., 1998]. Reflectivity data have been utilized in two formats. For real-time implementation, the Digital Hybrid Reflectivity (DHR) product has been utilized. An ftp protocol has been implemented for automatic transfer of the DHR product from NWS to Princeton at the completion of each volume scan. For post-analysis applications, we have used the Archive Level II volume scan reflectivity data from the National Climatic Data Center (NCDC). For rainfall estimation over Dead Run, which is approximately 70 km from the Sterling radar, the 0.5 degree elevation angle is used for both reflectivity products.

The Network Model has also been implemented for the 9.1 km^2 Moores Run watershed in northeastern Baltimore City (Fig. 1). Real-time simulations for Moores Run were carried out as a part of the BFFP during the summers of 2004 and 2005. BFFP analyses in Sections 4 and 5 focus on Dead Run due to the dense network of stream gages and rain gages.

3 Hydrologic Modeling

The Network Model is a distributed hydrologic model (Morrison and Smith 2001; Zhang et al. 2001; Giannoni et al. 2003; and Turner-Gillespie et al. 2003, Zhang and Smith, 2003; Smith et al. 2005a, Hicks et al. 2005, and Slutzman and Smith, 2006) that has been adapted for application to flash flood forecasting in the BFFP. The Network Model partitions the drainage basin into hillslope and channel components and represents discharge at the outlet of a drainage basin as:

$$Q(t) \;=\; \int_A M(t \;-\frac{d_0(x)}{v_0} - \frac{d_1(x)}{v_1}, x)\; dx \tag{1}$$

where Q(t) denotes discharge ($m^3\ s^{-1}$) at time t (s), A is the domain of the drainage basin, x is a point within A, $d_0(x)$ is the distance (m) from x to the channel network, v_0 is the overland flow velocity ($m\ s^{-1}$), $d_1(x)$ is the distance (m) along the channel from x to the basin outlet, v_1 is the channel flow velocity ($m\ s^{-1}$) and M(t,x) is the runoff rate ($m\ s^{-1}$) at time t and location x. The total flow distance from x to the basin outlet is $d_0(x) + d_1(x)$, the sum of the overland flow distance and the channel flow distance. The runoff rate M(t,x) ($mm\ h^{-1}$) at time t and location x is computed from the rainfall rate R(t,x) using the Green-Ampt infiltration model with moisture redistribution (Ogden and Saghafian, 1997). Implementation of the model requires specification of the rainfall field, soil hydraulic parameters, and the overland flow distance and channel flow distance functions (which are obtained from the extracted

drainage network).

The Network Model computes the travel times from each model grid cell to each location on the drainage network for which model hydrographs are desired. Computing travel times requires only the distance functions $d_0(x)$ and $d_1(x)$ and the velocity parameters v_0 and v_1. A lookup table of travel times is computed in a pre-processing step and used in model simulations. Knowing the travel time of each grid cell to a forecast point, means that discharge at any time t can be computed as the sum of runoff contributions from individual grid cells in the basin, using the appropriate lag times computed from the lookup table. There is no need for routing flow from grid cell to grid cell. This feature of the Network Model is the key to achieving run times that are suitable for flash flood applications in urban drainage basins. All of the software (rainfall pre-processing, Network Model and post-analysis displays) is included as a part of the final project report.

Model analyses in Section 5 use a reference set of model parameters that were obtained by modeling two flood events (Fig. 4) produced by short (15 minute) bursts of extreme rain rates. The 12 June 2003 event produced a 1.31 $m^3\ s^{-1}\ km^{-2}$ flood peak and a total runoff of 8 mm from a storm total rainfall accumulation of 17 mm (see Table 1) while the 5 November 2003 event produced a flood peak of 1.68 $m^3\ s^{-1}\ km^{-2}$ and a total runoff of 15 mm from a storm total rainfall accumulation of 23 mm. Model parameters used for simulating the 12 June 2003 and 5 November 2003 events are $v_0 = 0.088\ m\ s^{-1}$, $v_1 = 1.7\ m\ s^{-1}$, $K_s = 10\ mm\ h^{-1}$.

4 WSR-88D Rainfall Estimation

In this section, we examine WSR-88D rainfall estimates for 36 storms in the Dead Run watershed during the 2003 - 2005 observing period (Table 1). Volume scan reflectivity data from the Sterling WSR-88D were obtained for 23 storm events during the 2003 observing period, 12 events during the 2004 observing period and 1 event for the 2005 observing period. For each event, the basin-averaged storm total rainfall exceeded 5 mm. Storm total rainfall observations from the Dead Run rain gage network (Fig. 2) are used to examine the multiplicative bias in radar rainfall estimates and the capability of radar rainfall estimates to capture the spatial variation of rainfall for flash-flood producing storms. .

For the ith storm, $R_i(t, x)$ denotes the rainfall rate at time t, relative to the time origin U_i of the storm, and location x within the drainage basin. The domain of the basin is denoted A. The duration of the ith storm event is denoted T_i. The rainfall rate field for the ith storm is $\{R_i(t, x)\ ;\ t\ \in\ (0, T_i];\ x\ \in\ A\ \}$.

Rainfall rate fields $\{R_i(t, x)\}$ are estimated by applying a Z-R relationship ($R = aZ^b$; Z is the radar reflectivity factor in $mm^6\ m^{-3}$) to reflectivity observations at volume scan times $t_1, t_2, ...$ and for spatial locations $x_j; j = 1, ..., M$, where x_j denotes the center of the jth 1 degree by 1 km radar bin in the domain A and M is the number of radar bins. Analyses presented in this paper utilize the "convective" Z-R relationship for which a = 0.0174 and b = 0.71 and the "tropical" Z-R relationship

for which a = 0.010 and b = 0.83 (Fulton et al. [1998] and Baeck and Smith [1998]). The time-interpolated rainfall rate estimates at radar bin locations are given by linear weighting between volume scan times, i.e.,

$$\bar{R}_i(t, x_k) \;=\; \frac{t - t_j}{t_{j+1} - t_j}\; a[Z_i(t_{j+1}, x_k)]^b \;+\; \frac{t_{j+1} - t}{t_{j+1} - t_j}\; a[Z_i(t_j, x_k)]^b \tag{2}$$

for $t_j \;< t \;\leq t_{j+1}$. This computation provides estimates at an arbitrary time t, but for locations fixed to the center of radar sample bins x_k. The radar rainfall estimate for time t and location x, $\tilde{R}_i(t, x)$, is obtained by an inverse distance-squared weighting of the observations from radar bins:

$$\tilde{R}_i(t, x) \;=\; \sum_{k=1}^{M} w_k\; \bar{R}_i(t, x_k) \tag{3}$$

for

$$w_k \;=\; \frac{\frac{1}{||x - x_k||^2}}{\sum_{j=1}^{M} \frac{1}{||x - x_j||^2}}. \tag{4}$$

The sample bias, B_i, for the ith storm is the ratio of the mean storm total rainfall at rain gage stations to the mean storm total rainfall from radar at rain gage locations, i.e.

$$B_i \;=\; \frac{\sum_{j=1}^{m} G_{ij}}{\sum_{j=1}^{m} \int_0^{T_i} \tilde{R}_i(t, x_j)\; dt} \tag{5}$$

where m is the number of rain gage stations (typically 18 for the Dead Run rain gage analyses), x_j is the spatial location of the jth rain gage and G_{ij} denotes storm

total accumulation for the ith storm from the jth gage. Bias-corrected rainfall rate estimates are given by:

$$\hat{R}_i(t,x) \;=\; B_i \; \tilde{R}_i(t,x) \tag{6}$$

For operational rainfall algorithms (Fulton et al. 1998 and Smith and Krajewski 1991), the multiplicative bias is computed over much of the radar umbrella. The preceding analyses reflect a "local" bias correction (see also Seo and Breidenbach 2002), which may be useful for flash flood forecasting in urban regions with dense rain gage networks.

Multiplicative bias is a dominant component of the error in operational radar rainfall estimates (Smith et al. 1996). Storm event bias values for the convective Z-R relationship range from 0.52 to 2.14 for the 2003 events and from 0.41 to 2.77 for the 2004 events (Table 1). There is a pronounced seasonal variation in the multiplicative bias for the 23 events during 2003. Of the 11 events that occurred between 20 June and 1 September, 9 have bias values less than 1 (for the convective Z-R relationship). None of the 14 events outside this time window have bias values less than 1. For the 2004 observations, half of the 12 events, all of which occurred between 20 June and 1 September, have bias values less than 1.

Bias values are systematically larger for the major flood events (see also analyses of the 4 major urban flash flood events in the Philadelphia region in Section 6) . Bias

values for the ten largest flood peaks in 2003 were all greater than 1. Bias values for the two major flood events in 2004 were both greater than 1, 1.51 for the 7 July 2004 event and 1.35 for the 27-28 June 2004 event. The 28 June 2005 storm had a bias value of 1.2.

Seasonal variability in bias estimates reflects the relationship between bias and convective potential of the storm environment (Fig. 5). For storms during the 2003 observing period, the convective potential of the pre-storm environment was quantified through lifted index values computed from ETA model analysis fields (Black 1994; the ETA model has been renamed the North American Mesoscale model). Lifted index, which is defined as the difference between the 500 mb temperature and the temperature a surface parcel would have if lifted to 500 mb, provides a measure of convective potential in the pre-storm environment. Lifted index was computed from ETA model fields using the 2115 UTC model analysis preceding the storm event. Analyses suggest that unstable conditions over the region (average lifted index values less than 0) are associated with significant overestimation using the convective Z-R relationship. Highly stable environments can result in severe underestimation by the WSR-88D rainfall algorithms. Lifted index values between 2 and 5 are associated with bias values in the 1.1 - 1.6 range.

Radar rainfall estimates are strongly dependent on Z-R relationship, but there is relatively little difference in bias-corrected radar rainfall estimates between the convective and tropical Z-R relationships; see, for example, Figs. 6 and 7 in which storm

total rainfall estimates from tropical and convective Z-R relationships are compared with rain gage accumulations for the 12 June 2003 storm. The multiplicative bias values for the 2003 events using the tropical Z-R relationship ranged from 0.22 to 1.52 , with 6 of 23 values greater than 1 and 8 of 23 values less than 0.5 (compare with results in Tables 1 and 2 for the convective Z-R relationship). The standard error in bias-corrected radar rainfall estimates is smaller in 16 of 23 events using the convective Z-R relationship, reflecting a modest advantage for the exponent in the convective Z-R relationship relative to the exponent of the tropical Z-R relationship.

Flash flooding in urban drainage basins is typically tied to spatial variation of rainfall at scales from 1 - 100 km^2 and temporal variation at scales ranging from 1 minute - 2 hours. Two central questions for flash flood forecasting are: 1) How well can radar rainfall estimates resolve rainfall variability on these scales? and 2) How important is rainfall variability on these scales for flash flood response?

Flash-flood producing rainfall can exhibit large spatial variation over the 14.3 km^2 Dead Run basin. For the 12 June 2003 storm, which produced a flood peak with a unit discharge of 1.31 $m^3\ s^{-1}\ km^{-2}$, storm total rainfall derived from WSR-88D varied from less than 10 mm to more than 30 mm (Fig. 6). Bias-corrected rainfall estimates for this storm capture the spatial variability quite well (Fig. 7). The capability to represent spatial variation of rainfall at scales smaller than 14.3 km^2 varies significantly from event to event. WSR-88D rainfall estimates for flash flood producing storms on 18-19 September 2003 (Hurricane Isabel) exhibit spatial

variation (Fig. 8) that is not reflected in the rain gage observations (Fig. 9).

The correlation between storm total rainfall from gages and bias-corrected radar rainfall estimates (Tables 1 and 2) ranges from values less than 0 to values close to 1. The 18-19 September 2003 event has a correlation of -0.40 and the 7 July 2004 storm (see additional discussion below) also has a negative correlation. For the 12 June 2003 event (see Figs. 6 and 7) the correlation between storm total rainfall from gages and bias-corrected radar rainfall estimates is 0.94. Correlation values exceed 0.50 for 22 of the 35 events and they exceed 0.7 for 13 of 35 events.

Magnitude of flooding is not a good indicator of the capability of WSR-88D rainfall estimates to resolve the spatial variation of flash-flood producing rainfall over the 14.3 km^2 watershed. The correlation results are poor for several of the major flood events (7 July 2004 and 18-19 September 2003) and good for others (27-28 July 2004 and 28 September 2003).

Operational flash flood forecasting algorithms (Davis and Jendrowski 1996 and 1998) are based on the assumption that for a given catchment, basin-averaged rainfall rate at an appropriate time scale provides an accurate representation of flood response of the catchment. Peak discharge observations from the Franklintown and DR2 stream gages within the Dead Run watershed (Fig. 2; at basin scales of 14.3 and 1.6 km^2, respectively) are used to empirically examine the relationship between basin-averaged radar rainfall estimates and peak discharge (Network Model analyses are presented in the next section).

Bias-corrected, basin-averaged radar rainfall estimates at 1 hour time scale can provide accurate representations of peak discharge at the 14.3 km^2 scale of Dead Run (Fig. 10). If one knows the maximum 15 minute rainfall rate, there is still significant information about the peak discharge (Fig. 10) but information has been lost in reducing the time scale from 60 to 15 minutes. Similarly, increasing the time scale beyond 60 minutes decreases the information on peak discharge (figure not shown). The critical time scale for rainfall estimates varies with basin scale and for Dead Run at 14.3 km^2, the time scale is approximately 60 minutes (Fig. 4).

Reducing the spatial scale from 14.3 km^2 to 1.6 km^2 produces several qualitative changes in predictability of peak discharge (Fig. 11). The relationships between peak rainfall rate and peak discharge are weaker than for the larger spatial scale and errors in small-scale, short duration radar rainfall estimates will become a dominant source of error in flash flood forecasts. At the 1.6 km^2 scale of DR2, the response time of the basin is closer to 15 minutes than 60 minutes, yet the peak 60-minute rainfall rates actually result in a higher correlation with peak discharge than the maximum 15-minute rainfall rates.

The relative lack of dependence of flood response at a particular location on a stream channel to spatial variability of rainfall over the upstream drainage basin is tied in large part to the network structure of the basin (Smith et al. 2005b). Even for storms with large spatial variability in rainfall, the distribution of travel distances to the basin outlet is not markedly different from the case in which rainfall is uniformly

distributed over the basin (Smith et al. 2005b). From an operational flash flood forecasting perspective, spatial variability of rainfall within a basin is less important for predicting discharge at the basin outlet than temporal variability of rainfall.

Estimating extreme rainfall rates from weather radar observations is a particular challenge for flash flood forecasting (see discussion in Krajewski and Smith 2002). The 7 July 2004 storm produced the flood of record throughout much of the Dead Run watershed. The flood resulted from a 2 hour period of heavy rainfall (Fig. 12) which produced rainfall accumulations of more than 125 mm in Dead Run. A series of convective elements tracked over Dead Run from 1900 to 2100 UTC (Fig. 12), with convection organizing into a line which produced the period of peak rain rates in Dead Run from 2000 - 2030 UTC (Fig. 13).

Storm total rainfall from WSR-88D rainfall estimates shows a swath of heavy rainfall passing through Dead Run (Fig. 14). The rainfall distribution was tightly concentrated around Dead Run, reflecting the most extreme flooding observed in the Baltimore region. On the 14.3 km^2 scale, the WSR-88D rainfall estimates provided an excellent representation of flash flood producing rainfall.

Storm total rainfall estimates from radar (Fig. 14) show large gradients over Dead Run. These gradients are not, however, reflected in rain gage observations (Fig. 15). Like the 18-19 September 2003 storm (Fig. 8; see also Tables 1 and 2) the spatial pattern of heavy rainfall was not accurately reproduced by the WSR-88D rainfall estimates over the 14.3 km^2 basin. WSR-88D radar rainfall estimates capture the

distribution of extreme flood-producing rainfall at the 14.3 km^2 scale of Dead Run, but they do not accurately reflect the spatial variability of rainfall over the 14.3 km^2 watershed.

Raindrop spectra observations made with a Joss-Waldvogel disdrometer (located on the UMBC campus 4 km southeast of Dead Run) show large variability in microphysical processes over the course of the 7 July 2004 storm (Fig. 16). Rainfall rate estimates derived from the convective Z-R relationship show a period of serious overestimation followed by a period of underestimation. Overestimation is linked to relatively large values of mean drop diameter and small values of drop arrival rate (Fig. 16). The mean diameter of the DSD peaks at 4.2 mm on the leading edge of the line. At the same time (2036 UTC), the drop arrival rate is less than 1000 $drops\ m^{-2}\ s^{-1}$. Over the next 4 minutes, the drop arrival rate steadily increases to more than 3000 $drops\ m^{-2}\ s^{-1}$ and the mean diameter decreases to a value less than 3 mm. This 4-minute time period corresponds to the first sharp spike in rain rate to 100 $mm\ h^{-1}$. For the next 20 minutes, rainfall rate fluctuates between 50 and 100 $mm\ h^{-1}$ with much of the fluctuation in rain rate due to variations in drop arrival rate. The peak rainfall rate at 2049 UTC was associated with a drop arrival rate of 5000 $drops\ m^{-2}\ s^{-1}$.

Petersen et al. [1999] show that reflectivity-based rainfall estimates of flash flood producing rainfall can not accurately locate the core of heaviest rainfall when drop-size distributions exhibit the types of variability shown in Fig. 16. Areas that experience

anomalously large reflectivity values associated with large drops and relatively small number concentrations will be subject to overestimation. The cores of heavy rainfall produced by anomalously large number density values in the drop-size distribution will be areas in which reflectivity–based rainfall estimates underestimate the true values.

The fundamental problem is estimating rainfall rate from a single variable, reflectivity, in settings for which there are pronounced variations in drop-size distributions. Polarimetric measurements can markedly improve the situation. Using a modified version of the (Z, Z_{DR}) algorithm of Zhang et al. [2001] results in very accurate rainfall rate estimates for the 7 July 2004 storm (Fig. 17a), in comparison with estimates derived from the convective Z-R relationship (Fig. 17b). For the polarimetric algorithm, the rainfall estimates are equally good at the high end, as in the central and lower portion of the rain rate distribution (Fig. 17 a). Resolving the detailed spatial distribution of heavy rainfall over the 14.3 km^2 for storms like the 7 July 2004 storm will require polarimetric observations.

Despite errors in the storm total rainfall distribution over Dead Run, the bias-corrected WSR-88D rainfall estimates provide an accurate depiction of the flood potential for the 7 July 2004 storm (Fig. 12). Even for the 1.6 km^2 DR2 subwatershed, the rainfall WSR-88D rainfall estimates, especially at the 60 minute time scale, provide an accurate representation of the potential for extreme flooding.

The 28 June 2005 storm produced the second largest flood peak during the 2003

- 2005 period, 3.7 $m^3\ s^{-1}\ km^{-2}$ at 14.3 km^2. Flooding was most severe in DR1 and downstream in DR3, with unit discharge peaks decreasing from 28 $m^3\ s^{-1}\ km^{-2}$ at the 1.2 km^2 scale of DR1, to 15 $m^3\ s^{-1}\ km^{-2}$ at the 4.9 km^2 scale of DR3. Storm total rainfall in DR1 exceeded 75 mm for each of the 4 rain gages in and adjacent to DR1, with a maximum accumulation of 95 mm. Rainfall began in DR1 at approximately 2215 UTC and the duration of the storm was less than 1 hour. The bulk of rain fell in DR1 during a 20-minute window centered around 2300 UTC. The minimum rain gage accumulation over the Dead Run basin for the storm was less than 25 mm and was located close to the outlet of the basin at Franklintown.

WSR-88D rainfall estimates resolve the spatial pattern of storm total rainfall for the 28 June 2005 storm well, with largest accumulations in DR1 (Fig. 18) and minimum accumulations close to the outlet of the basin. The bias for the convective Z-R relationship is 1.2. The WSR-88D rainfall estimates capture the magnitudes of rainfall accumulation (Fig. 19) over all of the basin except DR1, where there is severe underestimation. For the four rain gages in DR1 the mean rainfall accumulation is 83 mm; the mean of the WSR-88D rainfall estimates for these four locations is 48 mm. Bias correction for this event results in slight increases in rainfall over the DR1 watershed, where there was severe underestimation. It also results in significant overestimation at 10 of the rain gage locations (Fig. 19).

Heavy rainfall in DR1 during the 20 minute period centered at 2300 UTC was produced by storm elements that were decreasing in convective intensity as they

passed over Dead Run (Fig. 20). From 2252 to 2257 the area with reflectivity values greater than 35 dBZ at the 10 degree elevation angle (approximately 16 km above ground level) decreases from 24 to 11 km^2. The area with reflectivity values greater than 20 dBZ at the 10 degree elevation angle decreased to 4 km^2 at 2302 and peak reflectivity at 10 degrees was less than 5 dBZ by 2307 UTC. The largest reflectivity values at 10 degree elevation angle for the storm occurred at 2211 UTC and exceeded 50 dBZ. Similar inferences follow from examining the changing reflectivity distribution at approximately 9 km AGL (5 degree elevation angle) The area with reflectivity values exceeding 50 dBZ decreased from 22 to 10 km^2 during the period 2252 - 2257 UTC. Reflectivity values greater than 65 dBZ were observed for the 5 degree elevation angle at 2211 UTC. These observations point to the large variation of reflectivity in the vertical and the need to measure reflectivity close to the ground.

The Terminal Doppler Weather Radar (TDWR) network provides one avenue for improving rainfall estimates for flash-flood producing storms in small urban watersheds (Smith et al. 2005d). Reflectivity observations from the BWI TDWR are used to estimate rainfall for the 28 June 2005 storm. Bias-corrected TDWR rainfall estimates capture the detailed spatial variation of rainfall over Dead Run (Fig. 21).

5 Model Results for Dead Run

Network Model simulations were performed for 10 events (see Table 3) to examine the capability of forecasting flash floods using WSR-88D rainfall estimates and simple distributed hydrologic models. Three variables were chosen to compare observed and model discharge. These are the peak magnitude, time to peak, and the runoff volume around the peak. The volume around the peak is taken as the total volume during the 60 minute time window centered on the peak discharge. Runoff volume is converted to depth (in mm) through division by the drainage area of the basin.

Model simulations were performed for the ten events using model parameters derived for the 12 June 2003 and 5 November 2003 events (Section 3) and a constant initial moisture content with $\theta = 0.25$ (the average of initial moisture content used for the 12 June 2003 and 5 November 2003 simulations; see Section 3). This reflects the typical setting of operational flash flood forecasting in which limited information is available for calibration and there is little capability to usefully represent dynamically varying initial moisture conditions.

Model flood peaks (Fig. 22) and runoff volumes (figure not shown) match observed peaks and volumes reasonably well. The coefficient of determination (R^2), which is a measure of the correlation between the observed and simulated hydrographs, is 0.80 for flood peaks and 0.90 for flood volumes.

Timing errors (Fig. 23) for model simulations of peak discharge range from -15

minutes (model peaks too slow) to +48 minutes (model peaks too fast). Errors in model forecasts of peak time are strongly dependent on discharge, with timing errors taking larger, positive values with increasing peak discharge (see additional discussion below). Timing errors depend solely on the GIUH parameters v_0 and v_1. They are largely insensitive to other model parameters and bias correction (Fig. 23).

Sensitivity to initial soil moisture is investigated by allowing the initial moisture content to vary from event to event (Fig. 24). The coefficient of determination increases from 0.81 to 0.96 for peak magnitude if soil moisture is calibrated for each event. For runoff volume, the coefficient of determination increases from 0.90 to 0.99. These results suggest some potential for improving peak forecasts through information on initial soil moisture conditions. In Smith et al. [2005b], it is shown that storm event runoff ratio in Dead Run varies systematically over the warm season (April - September), suggesting that seasonally varying initial moisture parameters could capture some of the improvement in peak forecasts reflected in the variable initial moisture condition simulations.

Bias correction of radar rainfall estimates is a key element of flash flood forecasting systems for small urban watersheds. The coefficient of determination decreases from 0.81 to 0.68 for the case of no bias correction. Bias varies systematically with event magnitude, with bias values for the largest events clustering around 1.4. Consequently, the effects of bias correction will vary with event magnitude.

Limitations of IUH-based models are apparent from model simulations for the

10 events. Hydraulic effects which are not accounted for in the Network Model (or other hydrologic models) are a source of errors in model analyses. The early rise of the simulated hydrographs compared to the observed hydrographs (Fig. 4) is one example. Flow velocities in stream channels (and storm sewers) are not constant over time, but vary with flow magnitude, as reflected in Manning's equation. The constant velocity assumption, which is critical for computational efficiency, reflects mean conditions during the central portion of the hydrograph. Flow velocities are lower during on the early portions of the flood, so the model hydrograph rises faster than the observed hydrograph.

During extreme flood events, significant flow volumes are conveyed by floodplains. For the major flood events in Dead Run, hydraulic processes associated with coupled channel-floodplain flow result in decreased flow velocities and significantly longer response times. Of particular importance in Dead Run are the effects of valley bottom constrictions associated with bridges and bridge abutments. In the DR3-DR4 reach, bridge crossings produce extensive areas of backwater for large floods. The storage effects of the DR3-DR4 reach explain the anomalously large flow attenuation at Franklintown for the three largest events, 7 July 2004, 27-28 July 2004, and 28 June 2005 (Fig. 25). For these three events, model simulations peak 18-48 minutes before the observed discharge peaks.

Model simulations overestimate peak discharge for the 27-28 July 2004 and 28 June 2005 flood peak (Fig. 25), both of which have unit discharge peaks that approach

4 m^3 s^{-1} km^{-2}. By contrast, model simulations underestimate the 18 m^3 s^{-1} km^{-2} peak for the 7 July 2004 flood (Fig. 25). Model performance for the 27-28 July 2004 and 28 June 2005 floods reflect shallow overbank flow conditions (based on field observations). The observed hydrograph for the 7 July 2004 event is similar to the 27-28 July and 28 June events up to 4 m^3 s^{-1} km^{-2} but the sharp rise to peak for the 7 July 2004 event reflects changing hydraulic conditions in which floodplain velocities increase with increasing floodplain flow depths. To captures these hydraulic aspects of flood response in flash flood forecasting systems requires both hydraulic models and detailed information on constrictions in valley bottoms.

Model simulations for the nested set of gauges with drainage areas ranging from 1.2 to 6.1 km^2 (see Figs. 26 - 28 on results for 13 August 2004, 17 August 2004 and June 28 2005) illustrate difficulties in pushing the spatial scale of site-specific flash flood forecasting systems below 10 km^2. Model errors are tied both to heterogeneities of basin response within the Dead Run basin and the difficulties of estimating rain rate accurately as the spatial scale decreases below 10 km^2 and the time scale of basin response decreases below 60 minutes.

There are systematic timing differences between the DR3 and DR4 subbasins of Dead Run. The most extreme case is the 13 August 2004 flood (Fig. 26) for which the model hydrograph at DR3 peaks 14 minutes before the observed peak and the DR4 model peak is 25 minutes after the observed peak. The DR3 basin includes significant areas developed after the implementation of stormwater management regulations. As

a consequence, there are numerous stormwater detention structures in the DR3 basin (Smith et al. 2005b and Nelson et al. 2005), which lead to a slower response than in DR4, which has few stormwater detention structures (Fig. 2). In addition, old residential development in DR4 is characterized by dense storm drain networks that rapidly concentrate runoff [Smith et al., 2005a]. Capturing the impacts of stormwater detention basins on flood response poses an especially difficult challenge in developing flash flood forecasting systems for urban drainage basins.

The interplay of stormwater management infrastructure and transportation infrstructure can have a marked impact of urban flood response. In the DR4 subbasin, response to rainfall is characterized by two distinct hydrograph peaks. For the 13 August 2004, 18 August 2004 and 28 June 2005 events (Figs. 26 -28), the DR4 hydrograph exhibits a double-peak response, despite the fact that flood-producing rainfall is concentrated during a single pulse of extreme rain rates. This aspect of basin response is tied to the structure of the storm drain network, and in particular the truncation of drainage into two separate units, one upstream of the Baltimore Beltway (represented by the DR5 observations), and the second downstream of the Beltway. The first peak in DR4 is from the local storm drain network, downstream of the Beltway; the second peak is from the DR5 portion of the watershed (note, in particular, the hydrographs for the 13 August 2004 event). Detailed information on the storm drain network is required to capture this aspect of storm event response and it will generally not be available for operational flash flood forecasting.

Model hydrographs for the headwater catchments DR1, DR2 and DR5 are overdispersed relative to observed hydrographs (Figs. 26 - 28). The same holds for the downstream stations at DR3 and DR4, but to a lesser degree. Accurate modeling of hydrographs at Franklintown can result from compensating errors at the upstream stations. For the 13 August 2004 case, for example, the relatively accurate timing and peak magnitudes at Franklintown are tied to the compensating timing errors at DR3 and DR4.

It is difficult to capture the detailed variation in flood response between DR3 and DR4. For the 13 August 2004 event, the unit discharge peak is 1.7 $m^3\ s^{-1}\ km^{-2}$ in DR4 and 0.9 $m^3\ s^{-1}\ km^{-2}$ in DR3. Model simulations reflect the difference in peak magnitudes with a 1.2 $m^3\ s^{-1}\ km^{-2}$ peak in DR4 and a 0.5 $m^3\ s^{-1}\ km^{-2}$ peak in DR3. The DR5 peak is 5 $m^3\ s^{-1}\ km^{-2}$ for August 13 versus 2 $m^3\ s^{-1}\ km^{-2}$ for August 18. Model simulations do not capture the DR5 origin of the August 13 peak. For August 18, DR3 has a 3.8 $m^3\ s^{-1}\ km^{-2}$ peak and DR4 a 1.6 $m^3\ s^{-1}\ km^{-2}$ peak. Model simulations in this case do not capture magnitude or timing of the DR1 peak. Model simulations for DR1 place the peak with the second pulse of rainfall. The DR3 simulation is reasonable only due to compensating errors from DR1 and DR2.

Simulation of the 28 June 2005 flood (Fig. 28) produces flood peaks that are too high for DR4 and too low for DR3. The underestimation in DR1 is even more severe than at the downstream DR3 station. The 28 June 2005 storm produced rainfall accumulations over the DR1 basin that approached 100 mm in less than 30 minutes,

based on four rain gage observations in and adjacent to DR1 (as described in the previous section). WSR-88D rainfall estimates were generally good for the 28 June 2005 storm (see discussion in Section 4), but they did not capture the peak rainfall in DR1. The role of bias adjustment for modeling extreme floods is illustrated by modeling flood peak response in Dead Run using WSR-88D rainfall estimates with: 1) bias correction based on the 18 rain gauges, 2) bias correction for DR1 using only the four DR1 gauges, and 3) no bias correction (Fig. 29). Results again illustrate the prominent role of bias correction for quantitative flash flood forecasting.

6 Analyses of Flash Flooding in Philadelphia

Hydrometeorological analyses of rainfall and flash flood response are presented for three drainage basins in the Philadelphia metropolitan region (Fig. 30): Wissahickon Creek (drainage area of 168 km^2), Pennypack Creek (129 km^2) and Little Neshaminy Creek (69 km^2). Analyses focus on major flood events resulting from Tropical Storm Allison (16-17 June 2001), Hurricane Floyd (16-17 September 1999), an extratropical cyclone on 16-17 October 1996 and a squall line-snowmelt event on 19-20 January 1996.

The largest flood peaks in the Philadelphia region were produced by Tropical Storm Allison and Hurricane Floyd (Fig. 31) and these peaks are much larger than preceding peaks in the region. For Wissahickon Creek at 168 km^2 (Lower Wissahickon

Creek in Fig. 30), the flood peak from Allison nearly doubled the third largest flood peak, but was only 65% of the flood peak from Hurricane Floyd in 1999. The difference between the peak magnitudes diminishes at the 106 km^2 scale of the U.S. Geological Survey (USGS) gaging station on Wissahickon Creek at Fort Washington (Upper Wissahickon in Fig. 30), from 405 m^3 s^{-1} to 311 m^3 s^{-1} . For Little Neshaminy Creek at 69.4 km^2, Allison produced a flood peak that was 25% larger than the peak from Floyd.

The most severe flooding from the four storms occurred in the upper Pennypack Creek at a basin scale of approximately 20 km^2 (Fig. 30) during Tropical Storm Allison. Flash flooding in the upper Pennypack Creek resulted in eight fatalaties. The USGS gaging station at Pennypack Creek malfunctioned during Allison, so direct comparison of the flood peaks from Allison and Floyd is not possible, even at the 106 km^2 scale of the basin above the USGS gaging station. We simulate the discharge time series in the upper Pennypack Creek basin using the Network Model and use these analyses to examine implementation of flash flood forecasting systems for extreme floods in ungaged urban catchments.

Volume scan WSR-88D reflectivity observations from the Fort Dix radar are used to examine high-resolution rainfall estimates for extreme flash flood producing storms in the Philadelphia metropolitan region. Rainfall analyses, based on WSR-88D volume scan reflectivity observations and rain gage observations, were performed for the 19-20 January 1996, 16-17 October 1996, 16-17 September 1999 and 16-17 June 2001

storms in the Philadelphia metropolitan region.

The January 1996 storm produced record and near-record flooding in the Susquehanna and Delaware River basins (Barros and Kuligowski 1998). Flooding in the Philadelphia metropolitan region resulted from a combination of snowmelt and anomalously high rainfall rates from a pre-frontal squall line that moved rapidly over the region. The October 1996 storm (Keim 1998) also had an extensive history of flooding in the northeastern United States. The storm produced record rainfall and flooding in southeastern Maine. Storm total accumulations of more than 800 mm were reported in Maine and resulted in several dam failures. Hurricane Floyd produced record flooding in North Carolina, eastern Pennsylvania and New Jersey. The prodigious rainfall totals were associated with the interaction of the tropical cyclone circulation with an extratropical system (see Atallah and Bosart 2003). The rainfall accumulation of 170 mm established a daily record for Philadelphia. Tropical Storm Allison was most noted for flooding in Texas and Louisiana (Bedient et al. 2003), but eight fatalities, numerous bridge failures and extensive property damage all occurred in a small section of Philadelphia.

Rainfall estimates at 1 km horizontal resolution and 5-minutes time scale were computed for each of the storms using volume scan reflectivity observations from the Fort Dix, New Jersey WSR-88D. Both convective and tropical ($R = 0.010Z^{0.83}$) Z-R relationships were examined. Storm total accumulations (Fig. 32) vary markedly between the tropical and convective Z-R relathionships. Peak rainfall accumulations

for Allison using the tropical Z-R relationship exceeded 600 mm, more than twice the peak accumulation values obtained from the convective Z-R relationship.

Bias adjustment of radar rainfall estimates was applied based on operationally available rain gage observations. Despite marked differences in storm properties, the bias estimates for the four storm events are quite similar. The convective Z-R consistently underestimated rainfall accumulations and the tropical Z-R overestimated rainfall accumulations. The relative magnitudes of overestimation (by the tropical Z-R) and underestimation (by the convective Z-R) are comparable. For the convective Z-R relationship, bias values were 1.53 (January 1996), 1.32 (October 1996), 1.41 (September 1999), and 1.35 (June 2001). The average bias for the four events using the convective Z-R relationship was 1.40. For the tropical Z-R relationship, the bias values were 0.78 (January 1996), 0.76 (October 1996), 0.77 (September 1999), and 0.64 (June 2001) for an average value of 0.74.

Bias-corrected storm total rainfall estimates for Tropical Storm Allison (Fig. 33) show little dependence on whether the initial rainfall estimates were derived with the convective or tropical Z-R relationship. This result implies that the difference in the exponent of the Z-R relationship, 0.71 versus 0.83, makes little difference in the storm total rainfall field. There are minor differences in temporal distribution of rainfall rates, but the general conclusion is that radar rainfall estimates are not overly sensitive to whether the convective or tropical Z-R relationship is chosen, provided that raingage observations are available for bias correction. Similar features

are observed for the other three events (figures not shown).

In implementing the Network Model, drainage networks for all the basins were extracted using digital elevation models (DEM) with 30 meter horizontal resolution. Accurate simulation of flood response in Little Neshaminy (Fig. 34) is obtained for tropical storm Allison using parameters $v_0 = 0.012\ m\ s^{-1}$ and $v_1 = 1.115\ m\ s^{-1}$ and $K_s = 6.0\ mm\ h^{-1}$.

Extreme rainfall from the the remnants of Tropical Storm Allisan was distributed across three basins, the upper portion of Pennypack Creek, Little Neshaminy Creek and the Sandy Run portion of Wissahickon Creek, as shown in Fig. 33 and described earlier. In each of these locations flood magnitudes were markedly larger for the 2001 event than for the 1999 event. The peak discharge in Little Neshaminy Creek was 320 $m^3 s^{-1}$ on 16 June 2001, which was 53 % larger than the reported peak discharge on 16 September 1999 (209 $m^3 s^{-1}$). The USGS reported high-water marks from the 1999 and 2001 floods. For sites in the upper Pennypack Creek, peak elevations for 16-17 June 2001 were 2-3 feet higher than flood peaks on 16 September 1999. The 2001 peak stages had return intervals ranging from 100 - 500 years based on FEMA floodplain maps. The 1999 peak stages in the upper Pennypack Creek had return intervals ranging from 10 - 100 years. All analyses point to the conclusion that flooding from the remnants of Tropical Storm Allison on 16-17 June 2001 was unprecedented in the core of heavy rainfall shown in Fig. 33, that is, in the Sandy Run, Little Neshaminy, and upper Pennypack Creek basins.

Storm total rainfall accumulations in the upper Pennypack Creek basin for the 16-17 June 2001 storm ranged from 250 to 350 mm with a basin-averaged rainfall accumulation of approximately 300 mm. Initial rainfall over the upper Pennypack Creek occurred around 1700 UTC. Over the course of the next 9 hours, embedded convective elements moved from southeast to northwest over the basin. Rainfall was concentrated in a 6-hour period beginning at 2000 UTC on 16 June 2001. The storm total accumulation in the upper Pennypack Creek basin was approximately twice the 100-year 12 hour rainfall accumulation for the region (Bonnin et al. 2004). Storm total accumulations for the 16-17 June 2001 storm were 50 - 100 mm greater than storm total rainfall accumulations for the 16 September 1999 storm in the upper Pennypack Creek basin.

The time series of discharge for upper Pennypack Creek was simulated for the 16-17 June 2001 storm using the Network Model with drainage network derived from a DEM and parameters derived for Little Neshaminy Creek (Fig. 35). Although there were no discharge estimates for use in validating the discharge time series, there were reports detailing the chronology and relative magntidues of flooding in upper Pennypack Creek.

The initial rise in upper Pennypack Creek on June 16 resulted from two pulses of rainfall around 1700 UTC and 1800 UTC. Significant flooding in upper Pennypack Creek, however, followed from a series of storm elements that passed over the area between 2000 UTC and 2130 UTC. These storm elements resulted in sharp rises in

upper Pennypack Creek after 2100 UTC. The sharp rise from 2130 to 2230 UTC resulted in flow in Pennypack Creek exceeding its channel capacity and entering the floodplain. Discharge in upper Pennypack Creek approached the magnitude associated with the 100-year floodplain (91 m^3s^{-1}; US COE 1973) by 2230 UTC. This chronology of events is consistent with reports from local residents and emergency response units that basement flooding in the area had begun by 2300 UTC. Rainfall over the upper Pennypack Creek basin was at relatively low magnitudes between 2130 and 2230 UTC resulting in a brief decrease in discharge around 2230 UTC. Flooding up until this time was significant, but the catastrophic nature of the flooding resulted from rainfall that began around 2230 UTC.

Discharge in the upper Pennypack Creek increased sharply and steadily from 2300 UTC (16 June) until 0200 UTC (17 June). The peak discharge occurred at approximately 0230 UTC June 17 and is estimated to have exceeded 170 m^3s^{-1} (Fig. 35). From 0200 until 0300 UTC, discharge in the upper Pennypack Creek hovered at values close to the peak discharge. Following 0300 UTC, discharge in upper Pennypack Creek receded steadily. The period between 0200 and 0300 UTC was the time period during which peak flooding (and fatalaties) occurred in the upper Pennypack Creek. The chronology of simulated flood response in upper Pennypack Creek matches the key elements of flood response from observer reports. High-resolution WSR-88D rainfall estimates and Network Model simulations provide a detailed depiction of the locating and timing of the most severe flooding from the 16-17 June 2001 storm in

Philadelphia.

References

Baeck, M. L. and J. A. Smith, 1998, Estimation of heavy rainfall by the WSR-88D, Weather Forecasting, Weather and Forecasting, 13, 416-436.

Black, T.L., 1994, The new NMC mesoscale Eta Model: Description and forecast examples. Wea. Forecasting, 9, 265-278.

Brandes, E. A., G. Zhang, and J Vivekanandan, 2004, Drop size distribution retrieval with polarimetric radar: Modle and Applications, J. of Applied Meteorology, 43, 461 - 475.

Burnash, R.J.C. (1995): The NWS river forecast system catchment modeling. In: Singh, V.P., (Ed.), Computer Models of Watershed Hydrology, Water Resources Publications, Littleton, CO, pp. 311-366.

Butts, M. B., J. T. Payne, M. Kristensen and H. Madsen. (2004). An evaluation of the impact of model structure on hydrological modelling uncertainty for streamflow prediction. Journal of Hydrology, Volume 298, Issues 1-4, 1 October 2004, Pages 242-266

Carpenter, T.M., and Georgakakos, K.P., 2004. Impacts of parametric and radar rainfall uncertainty on the ensemble streamflow simulations of a distributed hydrologic model. DMIP Special Issue of the Journal of Hydrology

Changon, S.A. 1999, Record flood-producing rainstorm of 17-18 July 1996 in the Chicago Metropolitan Area. Part III: impacts and responses to the flash flooding,

Journal of Applied Meteorology, Vol. 38, No. 3, pp. 273-280.

Ciach, J.G. and Krajewski, W.F., 1999, On the estimation of radar rainfall error variance, Advances in Water Resources, 22(6), 585-595.

Ciach, G. J., Habib, E., and W. F. Krajewski, 2003, Zero-covariance hypothesis in the error variance separation method of radar rainfall verification, Advances in Water Resources, 26, 573-580.

Davis, R.S., 1998, Detecting Time Duration of Rainfall: A Controlling Factor of Flash Flood Intensity, Special Symposium of the American Meteorological Society, Phoenix, AZ, pp. 258-263.

Davis, R.S., 1998, Flash Flood Forecasting, Conference on Severe Local Storms, Sponsored by the American Meteorological Society, Minneapolis, MN, Vol. 19, p. 395.

Davis, R. D. and P. Jendrowski, 1996, The operational Areal Mean Basin Estimated Rainfall (AMBER) module. Preprints 16 th Conf. on Weather Analysis and Forecasting, Norfolk, Amer. Meteor. Soc., 332- 335.

Davis, R. D. and P. Jendrowski, 1998, Detecting the time duration of rainfall: A controlling factor of flash flood intensity. Preprints Special Symposium on Hydrology, Phoenix, Amer. Meteor. Soc., 258-263.

Doswell, C.A. III, H.E. Brooks and R.A. Maddox, 1996, Flash flood forecasting: an ingredients-based methodology, Weather and Forecasting, Vol. 11, No. 4, pp.

560-581.

Duan, Q., S. Sorooshian, and V. Gupta (1992): Effective and Efficient Global Optimization for Conceptual Rainfall-Runoff Models. Water Resources Research, 28, 1015-1031.

Fulton, R. A., J. P. Breidenbach, D.-J. Seo, D. A. Miller and T. O'Bannon, 1998, The WSR-88D rainfall algorithm, Weather and Forecasting, 13, 377 - 395.

Georgakakos K.P., Seo, D-J, Gupta , H, Schaake, J. and Butts, M.B. (2004).Characterising streamflow simulation uncertainty through multimodel ensembles, Journal of Hydrology, Volume 298, Issues 1-4, 1 October 2004, Pages 222-241.

Giannoni, F., J. A. Smith, Y. Zhang, and G. Roth, Hydrologic modeling of extreme floods using radar rainfall estimates, Advances in Water Resources, 26, 195-203, 2003.

Gupta, H.V., S. Sorooshian, and P.O. Yapo (1998): Toward improved calibration of hydrologic models: Multiple and noncommensurable measures of information. Water Resources Research, 34, 751-763.

Gupta, V.K., E. Waymire, and C.T. Wang (1980): A representation of an instantaneous unit hydrograph from geomorphology. Water Resources Research, 16(5), 885-862.

Hicks, N. S., J. A. Smith, A. J. Miller, and P. A. Nelson, 2005, Catastrophic flooding from an orographic thunderstorm in the central Appalachians, Water Resour. Res., 41, W12428, doi:10.1029/2005WR004129.

Ivanov, V.Y., Vivoni, E.R., Bras, R.L. and Entekhabi, D. 2004. Preserving High-Resolution Surface and Rainfall Data in Operational-scale Basin Hydrology: A Fully-distributed Physically-based Approach. Journal of Hydrology. 298(1-4): 80-111.

Julien, P.Y., B. Saghafian, and F.L. Ogden (1995): Raster-based hydrological modeling of spatially-varied surface runoff. Water Resources Bulletin, 31(3), 523-536.

Koren, V., S. Reed, M. Smith, Z. Zhang, and D.-J. Seo (2004): Hydrology laboratory research modeling system (HL-RMS) of the US national weather service. Journal of Hydrology, 291, 297-318.

Krajewski W. F., Ciach G. J., and Habib E.H., 2003, An analysis of small-scale rainfall variability in different climatic regimes, Journal of Hydrological Sciences, 48, 151-162.

Krajewski, W. F. and J. A. Smith, 2002, Radar hydrology: rainfall estimation, Advances in Water Resources, 25, 1387 1394.

Morrison, J. E. and J. A. Smith, Scaling properties of flood peaks, Extremes, 4(1), 5 - 23, 2001.

Nelson, P. A. , J. A. Smith and A. J. Miller, Evolution of channel morphology and hydrologic response in an urbanizing drainage basin, Earth Surface Processes and Landforms, to appear.

Ogden, F. L. and B. Saghafian (1997): Green and Ampt Infiltration with Redis-

tribution. Journal of Irrigation and Drainage Engineering, ACSE, 123, 386-393.

Ogden, F. L., H. O. Sharif, S. Senarath, J. Smith, M. L. Baeck, and J. Richardson, 2000, Hydrologic Analysis of the Fort Collins, Colorado, Flash Flood of 1997, J. of Hydrology, 228, 82-100.

Petersen, W.A., L.D. Carey and S.A. Rutledge, 1999, Mesoscale and radar observations of the Fort Collins flash flood of 28 July 1997, Bulletin of the American Meteorological Society, Vol. 80, No. 2, pp. 191-216.

Reed, S., Koren, V., Smith, M., Zhang, Z., Moreda, F., Seo, D.-J. and DMIP Participants. 2004. Overall Distributed Model Intercomparison Project Results. Journal of Hydrology. 298(1-4): 27-60.

Smith, M.B., Koren, V., Pan, J.J., Zhang, Z. , 2004b. Runoff response to spatial variability in precipitation: An analysis of observed data. Journal of Hydrology DMIP Special Issue,

Seo, D.-J. and J. P. Breidenbach, 2002, Real-time correction of spatially nonuniform bias in radar rainfall data using rain gauge measurements, Journal of Hydrometeorology: Vol. 3, No. 2, pp. 93111.

Slutzman, J. E. and J. A. Smith, Effects of flood control structures on flood response for Hurricane Floyd in the Brandywine Creek watershed, Pennsylvania, ASCE J. of Hydrologic Engineering, in press.

Smith, J. A., D.-J. Seo, M. L. Baeck, and M. D. Hudlow, 1996, An intercomparison

study of NEXRAD precipitation estimates, Water Resources Research, 32(7), 2035 - 2045.

Smith, J. A. and W. F. Krajewski, 1991, Estimation of the mean field bias of radar rainfall estimates, Journal of Applied Meteorology, 30(4), 397 - 412.

Smith, J. A., M. L. Baeck, J. E. Morrison, P. L. Sturdevant-Rees, D. F. Turner-Gillespie and P. D. Bates, 2002, The regional hydrology of extreme floods in an urbanizing drainage basin, J. of Hydrometeorology, 3(3), 267 282.

Smith, J. A., A. J. Miller, M. L. Baeck, P. A. Nelson, G. T. Fisher, and K. L. Meierdiercks, 2005a, Extraordinary flood response of a small urban watershed to short duration convective rainfall, J. of Hydrometeorology, Vol. 6, No. 5, pages 599617.

Smith, J. A., M. L. Baeck, K. L. Meierdiercks, P. A. Nelson, A. J. Miller, and E. J. Holland, 2005b, Field studies of the storm event hydrologic response in an urbanizing watershed, Water Resources Research, 41, W10413.

Smith, J. A., M. L. Baeck, K. L. Meierdiercks, A. J. Miller and W. F. Krajewski, (2005c), Radar rainfall estimation for flash flood forecasting in small urban watersheds, submitted to Advances in Water Resources.

Steiner, M., J. A. Smith, S. J. Burges, C. V. Alonso, and R. W. Darden, 1999, Effect of bias adjustment and rain gage data quality control on radar rainfall estimates, Water Resources Research, 35, 2487 - 2503.

Turner-Gillespie, D. F., J. A. Smith and P. D. Bates, Attenuating reaches and the

regional flood response of an urban drainage basin, Advances in Water Resources, 26, 673 684, 2003.

Ulbrich, C. W. and D. Atlas, 1984, Assessment of the contribution of differential polarizatin to improved rainfall estimation, Radio Science, 19, 1, 49 - 57.

Vieux, B.E. and P.B. Bedient, 2004, Assessing Urban Hydrologic Prediction Accuracy Through Event Reconstruction, J. of Hydrology, 299(3-4), 217-236.

Vieux, B.E. (2001). Distributed Hydrologic Modeling Using GIS, Water Science and Technology Series, vol. 38. Kluwer, Norwell, MA, 293 pp. ISBN 0-7923-7002-3.

Vieux, B.E., Z. Cui, and A. Gaur (2004): Evaluation of a physics-based distributed hydrologic model for flood forecasting. Journal of Hydrology, 298, 155-177.

Vrugt, J.A., C.G.H. Diks, H.V. Gupta, W. Bouten, and J.M. Verstraten (2005): Improved treatment of uncertainty in hydrologic modeling: Combining the strengths of global optimization and data assimilation. Water Resources Research, 41, W01017, doi: 10.1029/2004WR003059.

Zhang, Y., J. A. Smith, and M. L. Baeck, The hydrology and hydrometeorology of extreme floods in the Great Plains of eastern Nebraska, Advances in Water Resources, 24(9-10), 1037 1050, 2001.

Zhang, Y. and J. A. Smith, 2003, Space-time variability of rainfall and extreme flood response in the Menomonee River basin, Wisconsin, J. of Hydrometeorology, 4, 506 - 517.

Zhang, G., J. Vivekanandan, and E. Brandes, 2001: A method for estimating rain rate and drop size distribution from polarimetric radar measurements. IEEE Trans. Geosci. Remote Sens., 39, 830841.

Date	Mean Rain (mm)	Max Rain (mm)	Bias	Correlation	Max 60 Rain $mm\ h^{-1}$	Peak Discharge $m^3\ s^{-1}\ km^{-2}$
June 3	17.1	17.9	1.43	0.28	3.1	0.26
June 7	38.1	41.9	1.97	0.43	10.6	1.71
June 12a	17.2	34.3	1.13	0.94	12.7	1.31
June 12b	11.3	25.5	0.59	0.96	4.7	0.47
June 17	13.7	15.2	2.14	0.66	6.3	0.49
June 19a	10.6	12.8	1.02	0.28	7.3	0.81
June 19b	8.6	9.9	0.81	0.61	4.2	0.49
July 2	34.9	41.7	1.57	0.11	8.9	0.63
July 7	5.2	15.6	0.79	0.77	3.5	0.26
July 23	23.6	27.7	1.42	0.56	13.1	0.93
July 28	7.1	8.8	0.77	0.04	3.3	0.11

Table 1. Storm event summaries for the 25 events during the 2003 observing period with storm total rainfall accumulation exceeding 5 mm, including: storm date, storm total rainfall (mm), maximum point rainfall accumulation over the basin (mm), bias (convective Z-R), correlation between radar and rain gage storm total accumulations (at rain gage locations), maximum 60-minute basin-averaged rainfall rate, and peak discharge of Dead Run at the Franklintown stream gage (expressed as a unit discharge, i.e. discharge divided by drainage area).

Date	Mean Rain (mm)	Max Rain (mm)	Bias	Correlation	Max 60 Rain $mm\ h^{-1}$	Peak Discharge $m^3\ s^{-1}\ km^{-2}$
August 3	8.7	13.2	0.63	0.54	3.7	0.24
August 9	9.9	15.8	0.95	0.79	10.5	0.70
August 11	5.0	13.0	0.95	0.82	5.0	0.31
August 16	15.7	21.5	0.70	0.77	7.6	0.36
August 22	10.9	21.6	0.52	0.41	11.7	0.59
Septem. 1	5.2	16.3	0.72	0.83	5.1	0.17
Septem. 12	26.7	29.0	1.91	-0.16	5.1	0.37
Septem. 18	64.9	73.7	1.51	-0.40	25.4	2.77
Septem. 22	73.3	85.7	1.47	0.91	26.5	3.31
October 14	41.3	48.0	1.83	0.50	16.9	1.78
October 27	53.9	56.6	1.36	0.59	10.6	1.45
Novemb. 5	22.5	28.0	1.15	0.71	17.1	1.68

Table 1. (continued)

Date	Mean Rain (mm)	Max Rain (mm)	Bias	Correlation	Max 60 Rain $mm\ h^{-1}$	Peak Discharge $m^3\ s^{-1}\ km^{-2}$
July 1	6.4	15.4	0.41	0.48	6.9	0.21
July 4	8.5	10.2	0.96	0.62	5.9	0.22
July 7	123	138	1.51	-0.05	79.3	9.0
July 18	6.7	10.0	1.63	0.83	1.6	0.07
July 23	25.9	35.3	1.19	0.43	17.3	1.52
July 28	48.1	63.5	1.35	0.87	36.2	3.67
August 1	11.8	17.5	0.58	0.05	5.3	0.72
August 4	17.4	22.9	2.77	0.64	16.3	0.72
August 11	11.5	16.4	0.70	0.58	12.0	0.79
August 12	5.8	9.1	1.26	0.81	10.2	1.18
August 18	20.9	41.9	0.85	0.97	15.8	1.30

Table 2. Storm event summaries for the 2004 observing period with storm total rainfall accumulation exceeding 5 mm, including: storm date, storm total rainfall (mm), maximum point rainfall accumulation over the basin (mm), bias (convective Z-R), correlation between radar and rain gage storm total accumulations (at rain gage locations), maximum 60-minute basin-averaged rainfall rate, and peak discharge of Dead Run at the Franklintown stream gage (expressed as a unit discharge, i.e.

discharge divided by drainage area).

Date	Rainfall [mm]	Runoff [mm]	Infiltration [mm]	Lag time (minutes)	Runoff Ratio
2003 12 June	17	8	9	54	0.47
2003 5 November	23	15	8	61	0.65
2004 7 July	123	87	36	100	0.71
2004 23 July	26	6	13	45	0.23
2004 27 July	48	24	24	75	0.50
2004 4 August	17	3	14	50	0.11
2004 11 August	12	3	9	55	0.25
2004 13 August	8	6	2	50	0.75
2004 17 August	21	11	10	60	0.52
2005 28 June	50	24	26	83	0.48

Table 3 Water balance summary for 10 events used for Network Model analyses. Infiltration is assumed to be the residual between the rainfall and the runoff. Lag time is defined as the difference between the time of peak discharge and the peak of the basin-averaged rainfall rate time series. The runoff ratio is the ratio of runoff to rainfall.

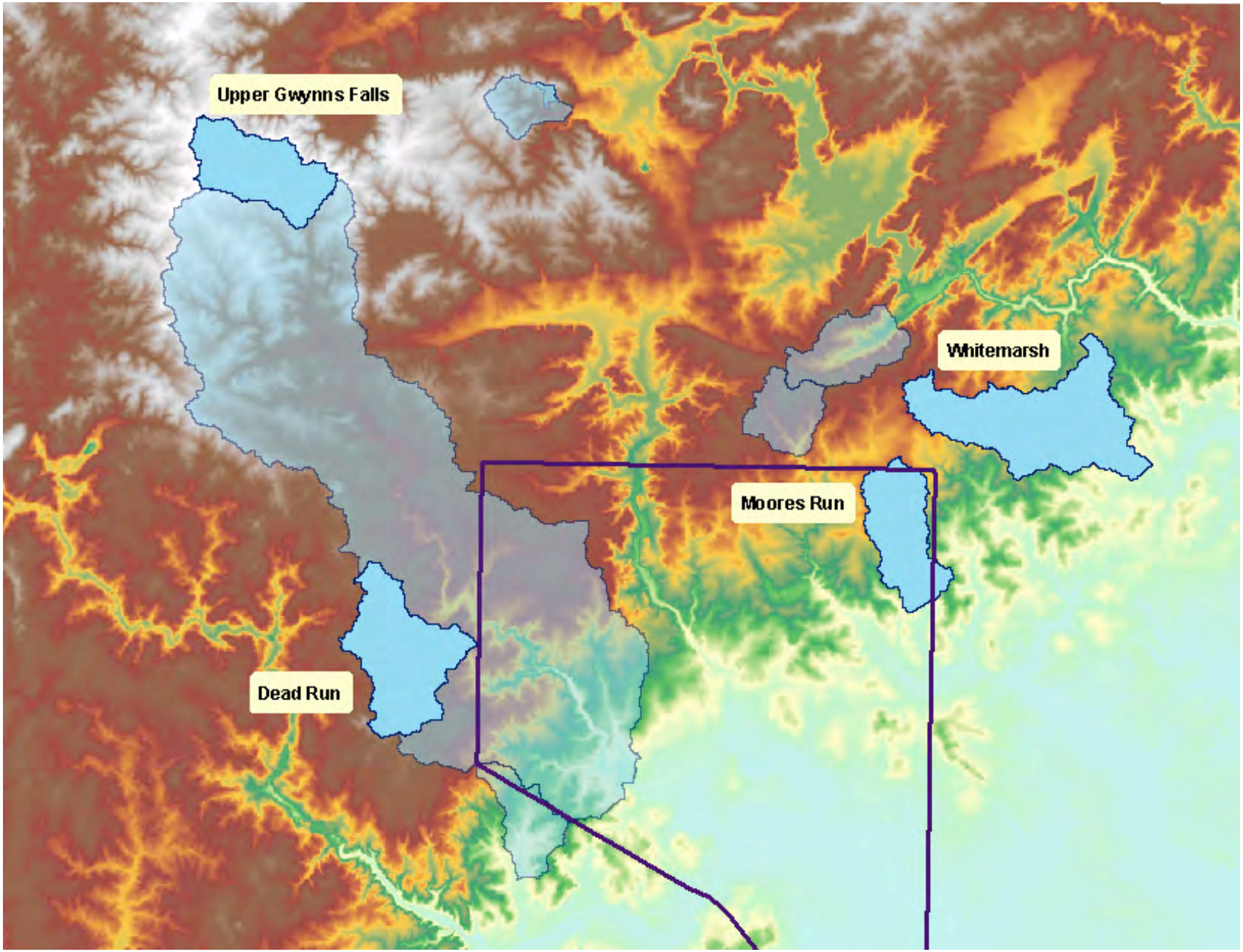

Figure 1. Baltimore study watersheds for the BFFP. The Gwynns Falls watershed is shaded in light blue. The Baltimore City boundary is outlined in purple.

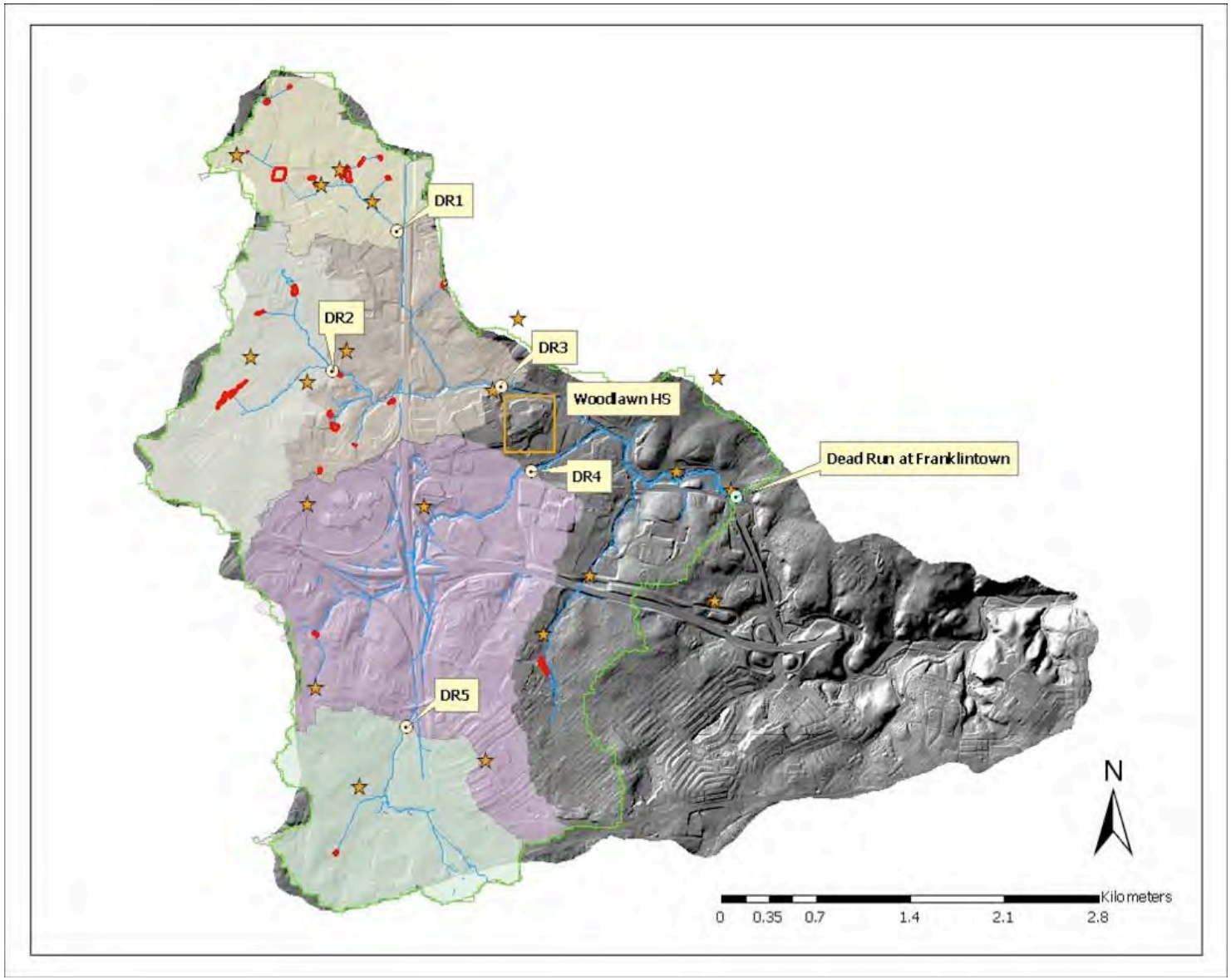

Fig. 2. The topography of the Dead Run watershed. Surface stream network is shown in blue lines. Basin boundaries for the five internal gauges are shown. Rain gauge locations are indicated by stars. Detention ponds are in shown in red.

Figure 3. Rain gage and stream gaging stations in the BFFP: Security Mall rain gage station (upper left), direct discharge measurement at DR5 (upper right) and downloading data logger at DR2 (bottom right).

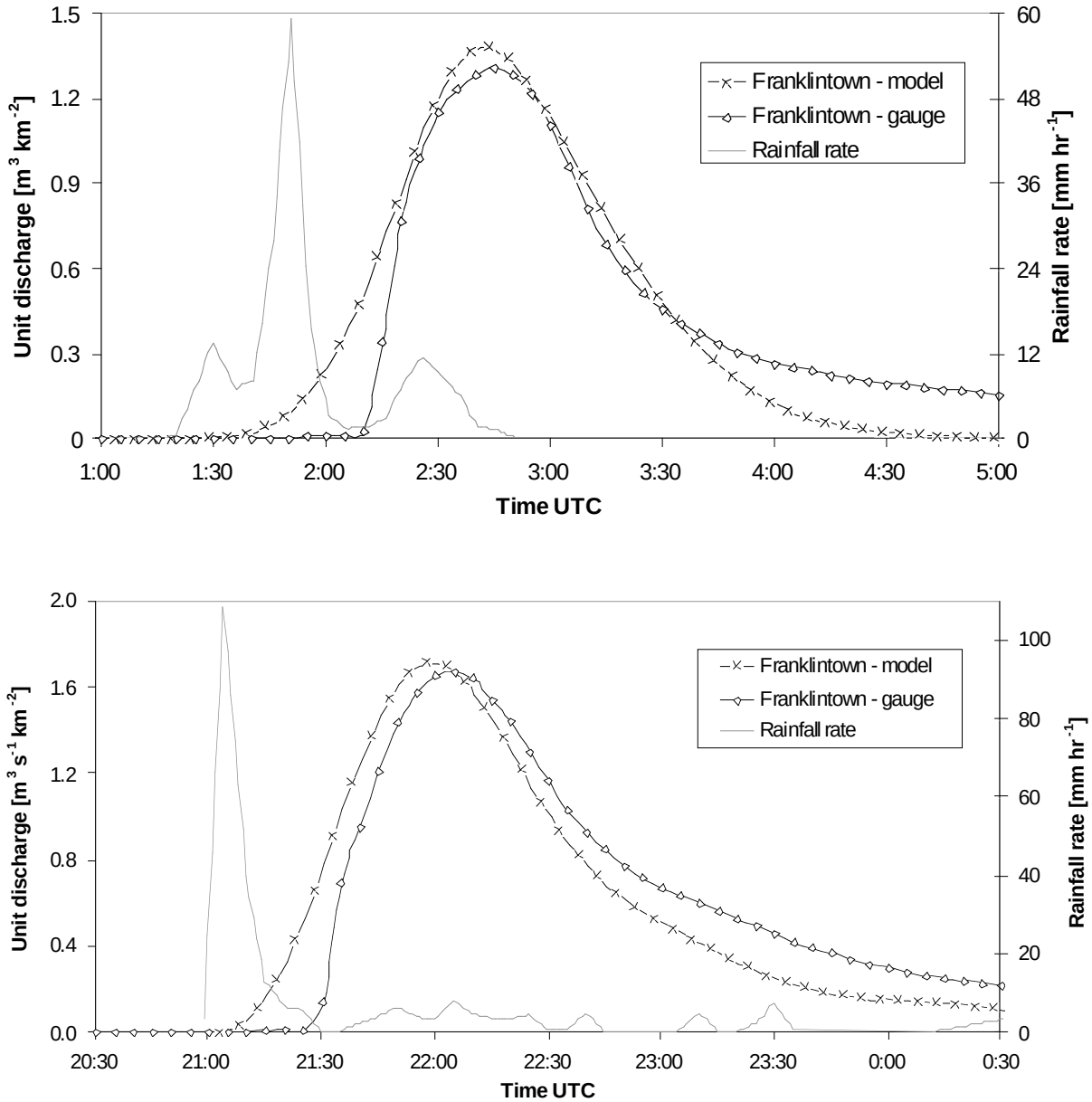

Figure 4. Comparison between observed and modeled discharge at Franklintown showing early rise of the hydrograph for: 12 June 2003 with v_0 = 0.088 m s^{-1}, v_1 = 1.7 m s^{-1}, K_S = 10 mm hr^{-1}, θ = 0.11 (top) and 5 November 2003 with v_0 = 0.088 m s^{-1}, v_1 = 1.7 m s^{-1}, K_S = 10 mm hr^{-1}, θ = 0.25 (bottom).

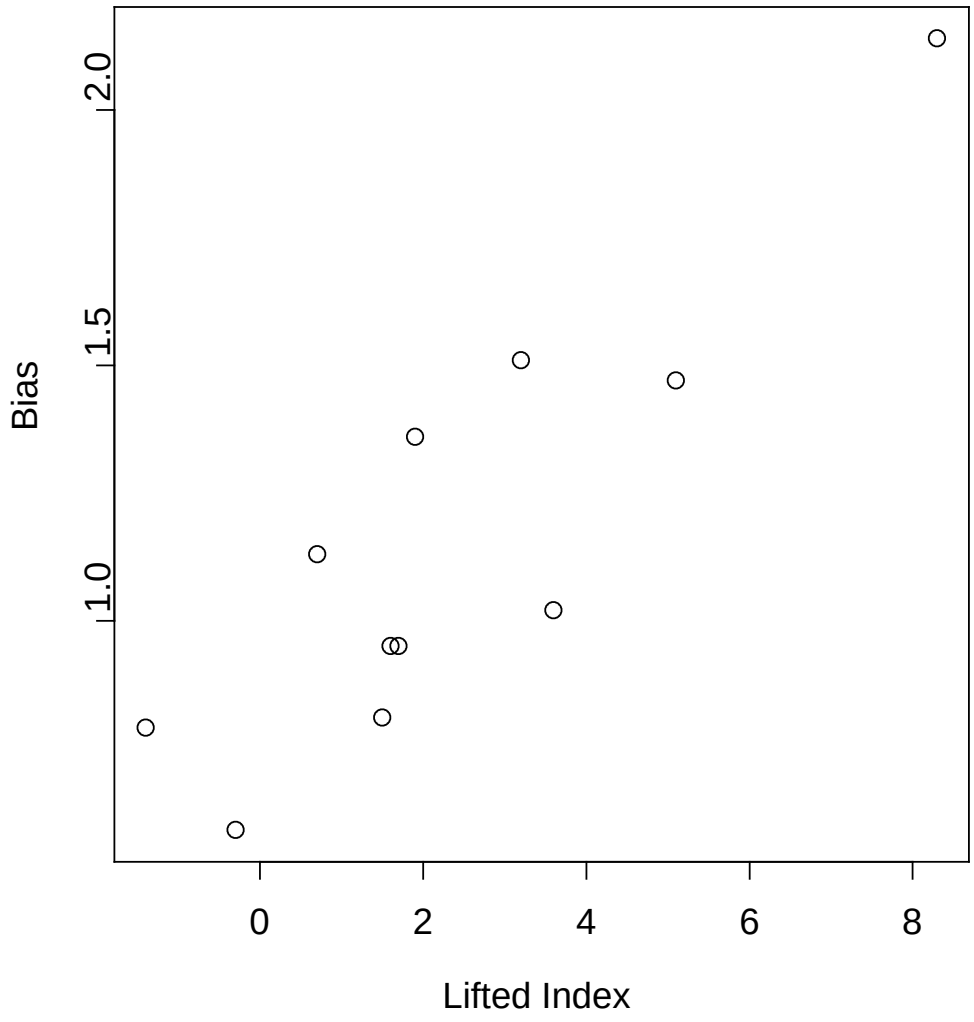

Fig. 5. Multiplicative bias vs pre-storm lifted index derived from 2115 UTC ETA model fields

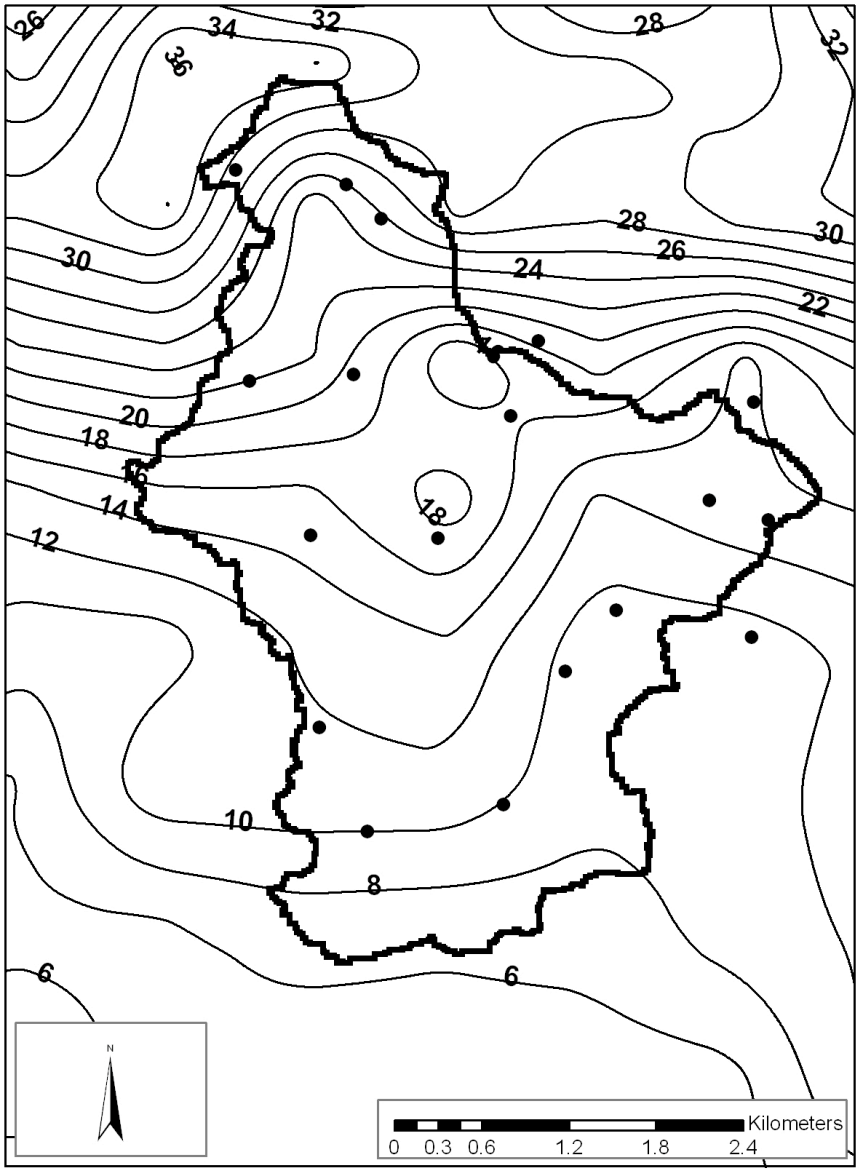

Fig. 6. Storm total accumulation (mm) for the 12 June 2003 storm (Dead Run boundary is shown).

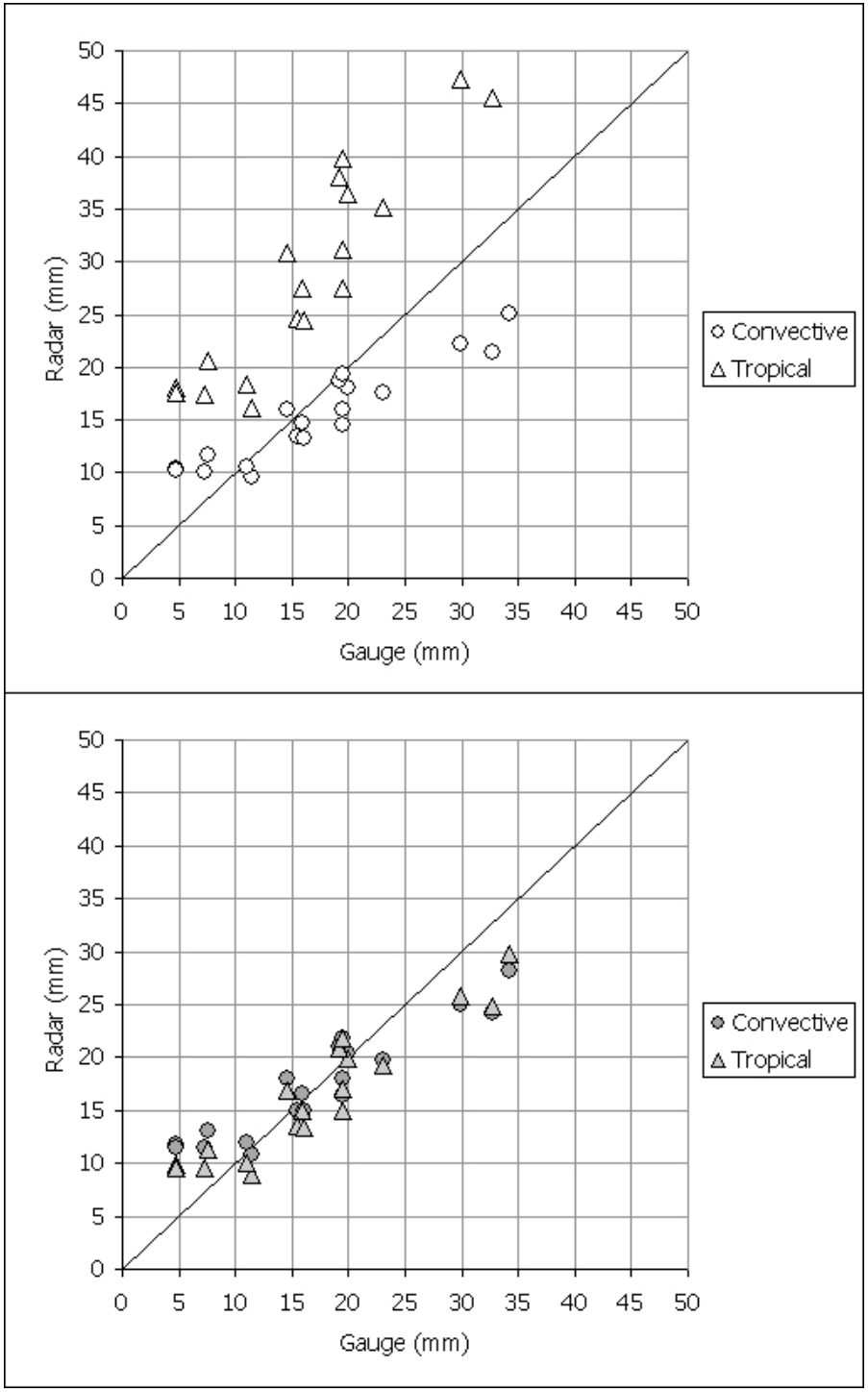

Fig. 7. Gage radar plot of storm total accumulation scatterplots (top figure is without bias correction; bottom figure is with bias correction)

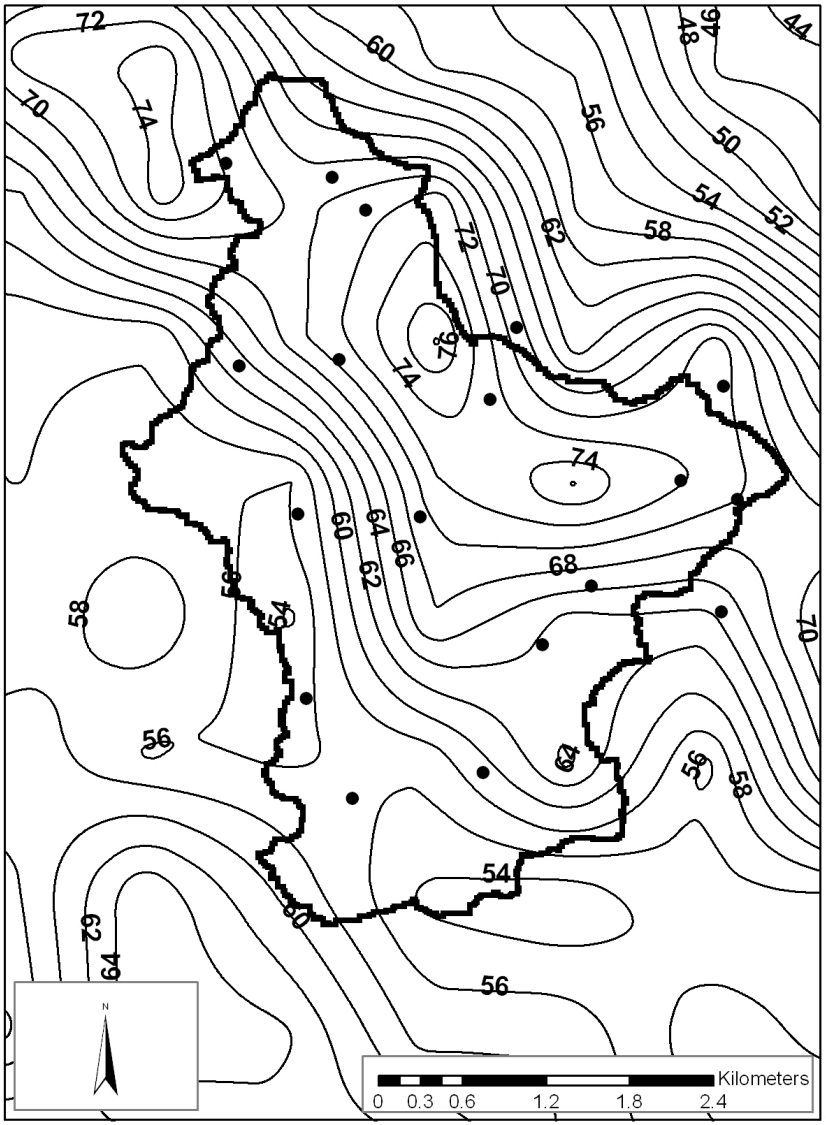

Fig. 8. Storm total accumulation (mmm) for 18 September 2003 storm (Dead Run boundary is shown).

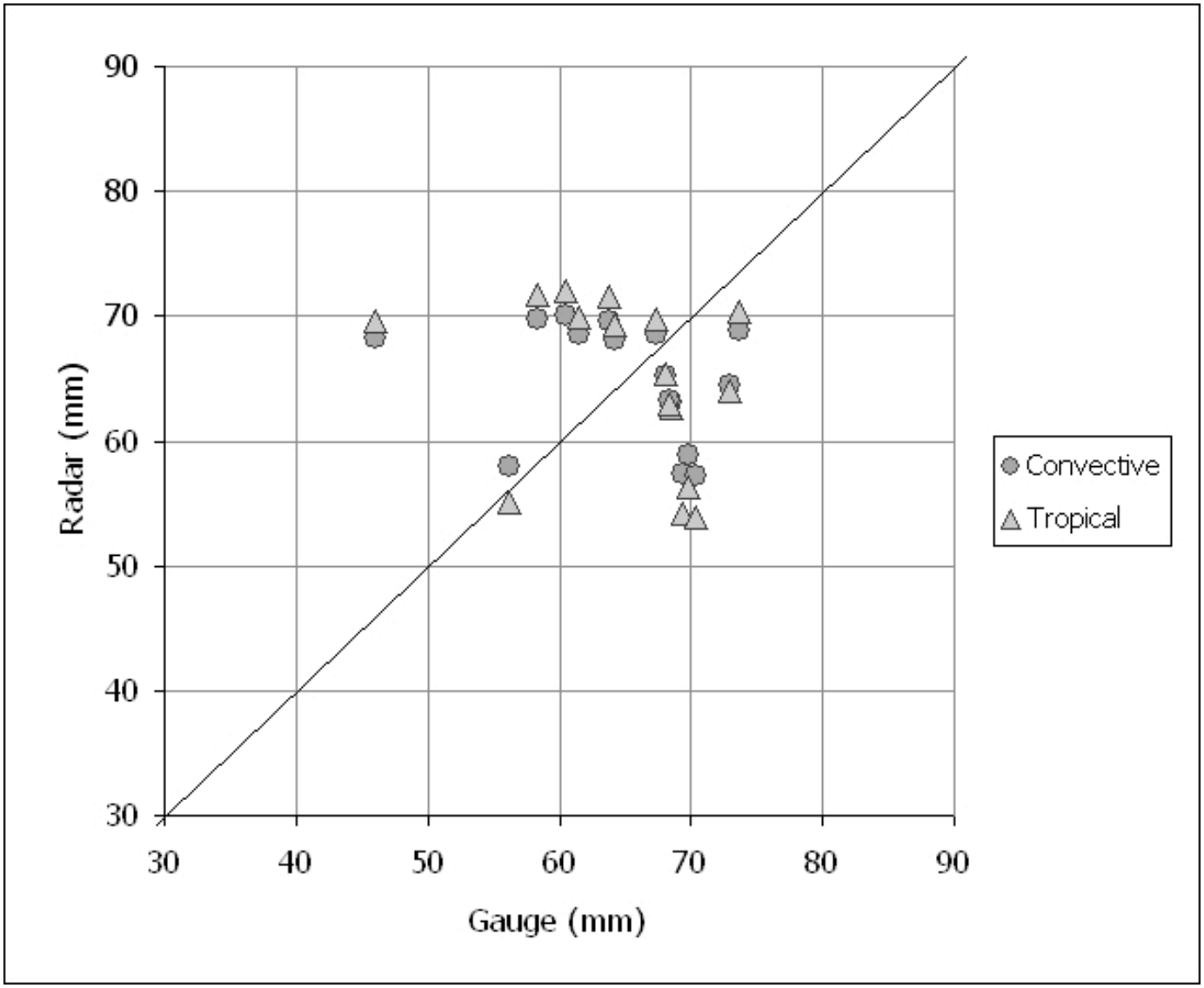

Fig. 9. Bias-corrected gage-radar scatterplots for the 18-19 September 2003 storm using both the convective and tropical Z-R relationships.

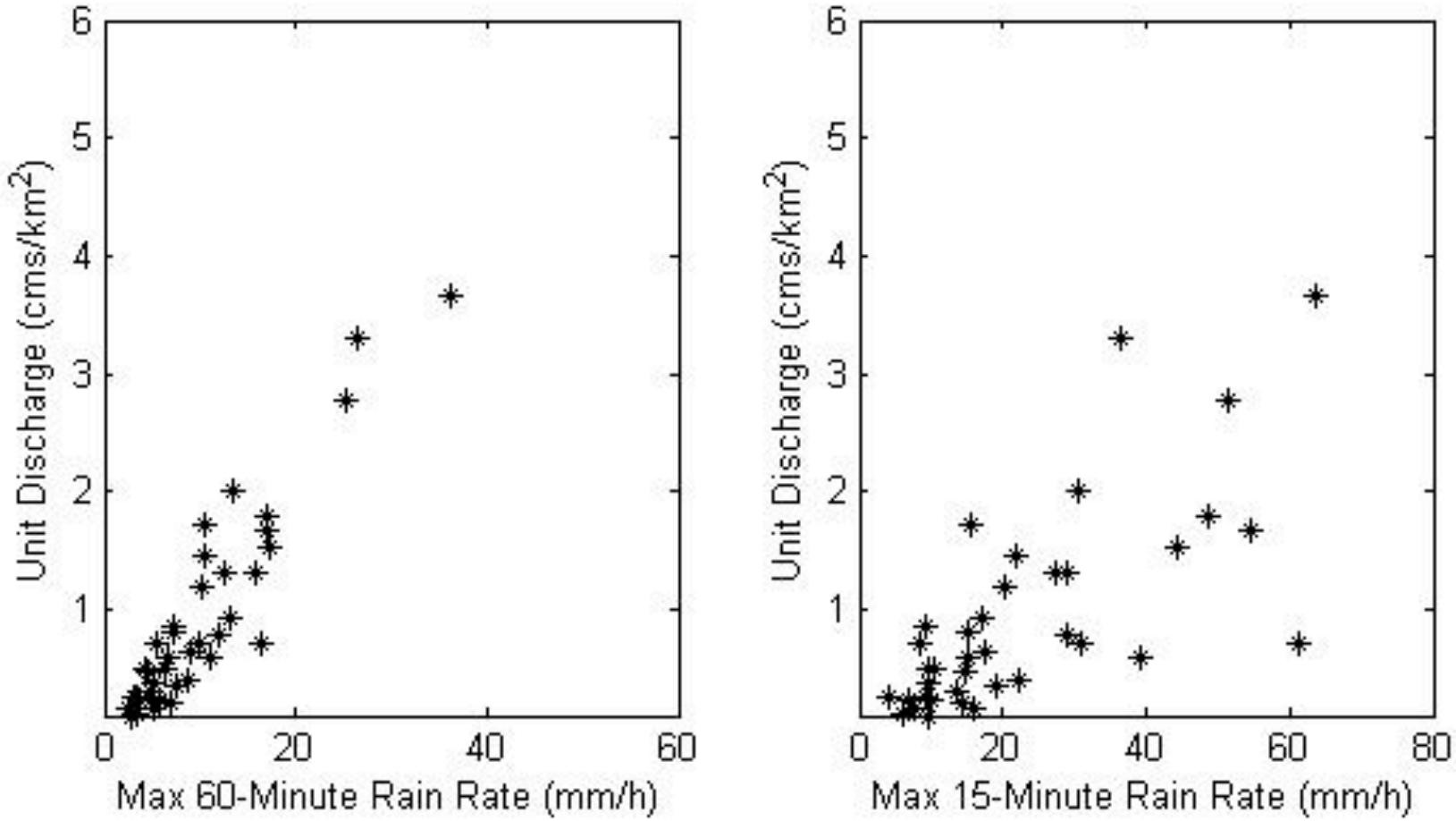

Fig. 10. Scatterplot of: a) maximum 60 minute rainfall rate vs. peak discharge (expressed as a unit discharge, i.e. $m^3\ s^{-1}\ km^{-2}$)for Dead Run at Frannklintown (14.3 km^2) and b) maximum 15 minute rainfall rate vs. peak discharge for Dead Run.

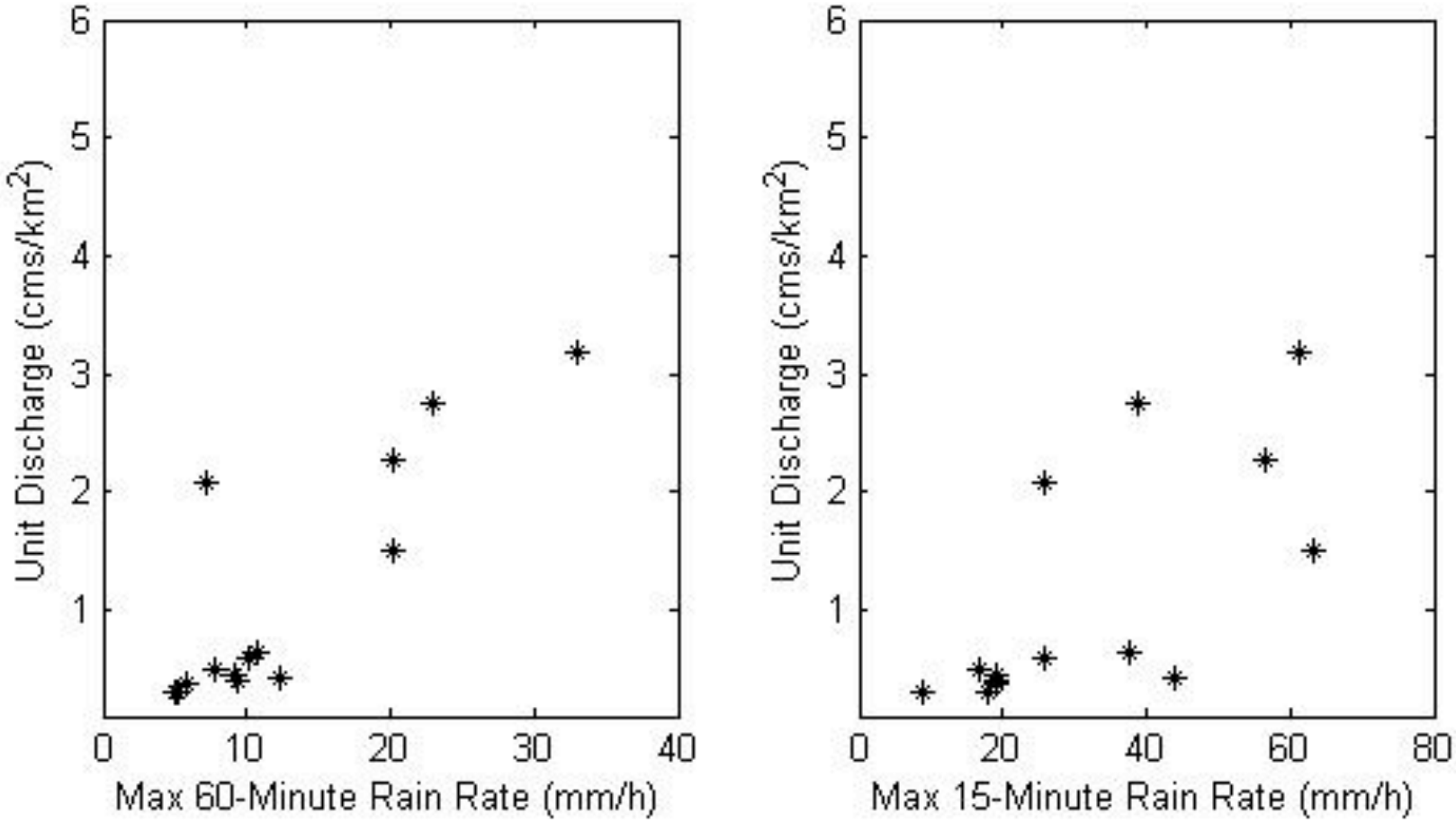

Fig. 11. Scatterplot of: a) maximum 60 minute rainfall rate vs. peak discharge (expressed as a unit discharge, i.e. $m^3\ s^{-1}\ km^{-2}$) for DR2 (1.6 km^2) and b) maximum 15 minute rainfall rate vs. peak discharge for Dead Run.

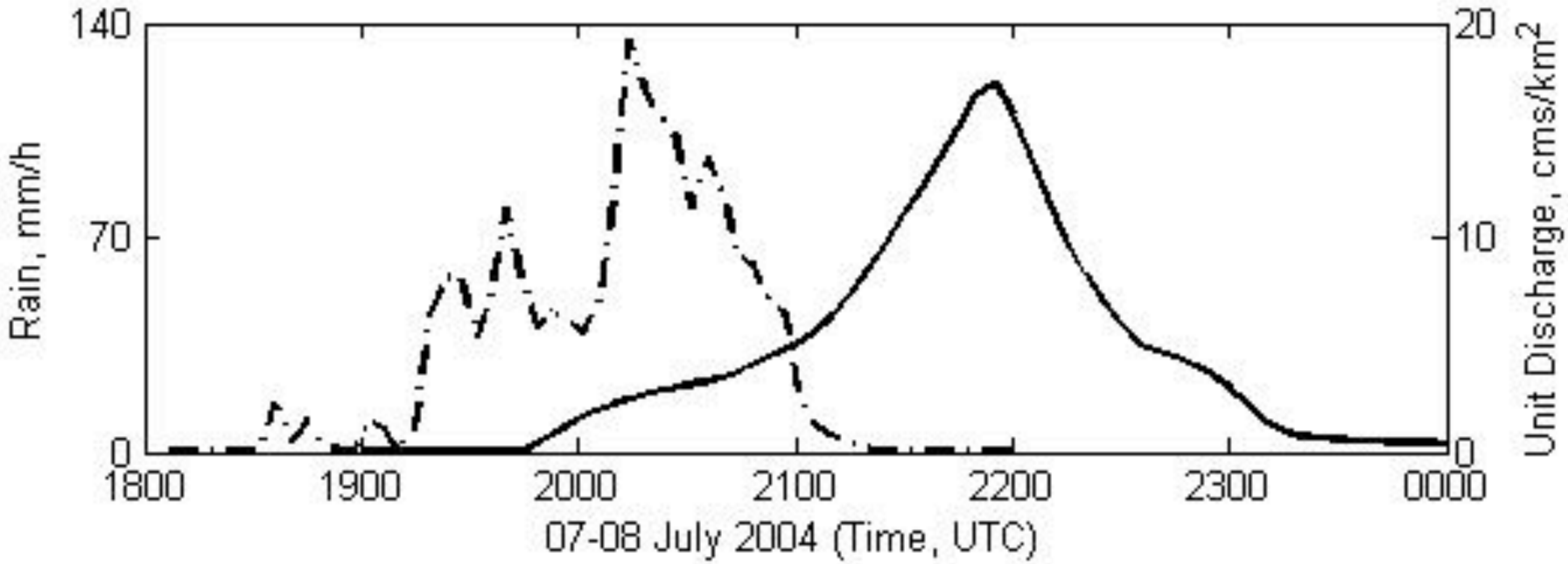

Fig. 12. Time series of basin-averaged rainfall rate and discharge (expressed as a unit discharge) for Dead Run at the Franklintown gage for the 7 July 2004 event.

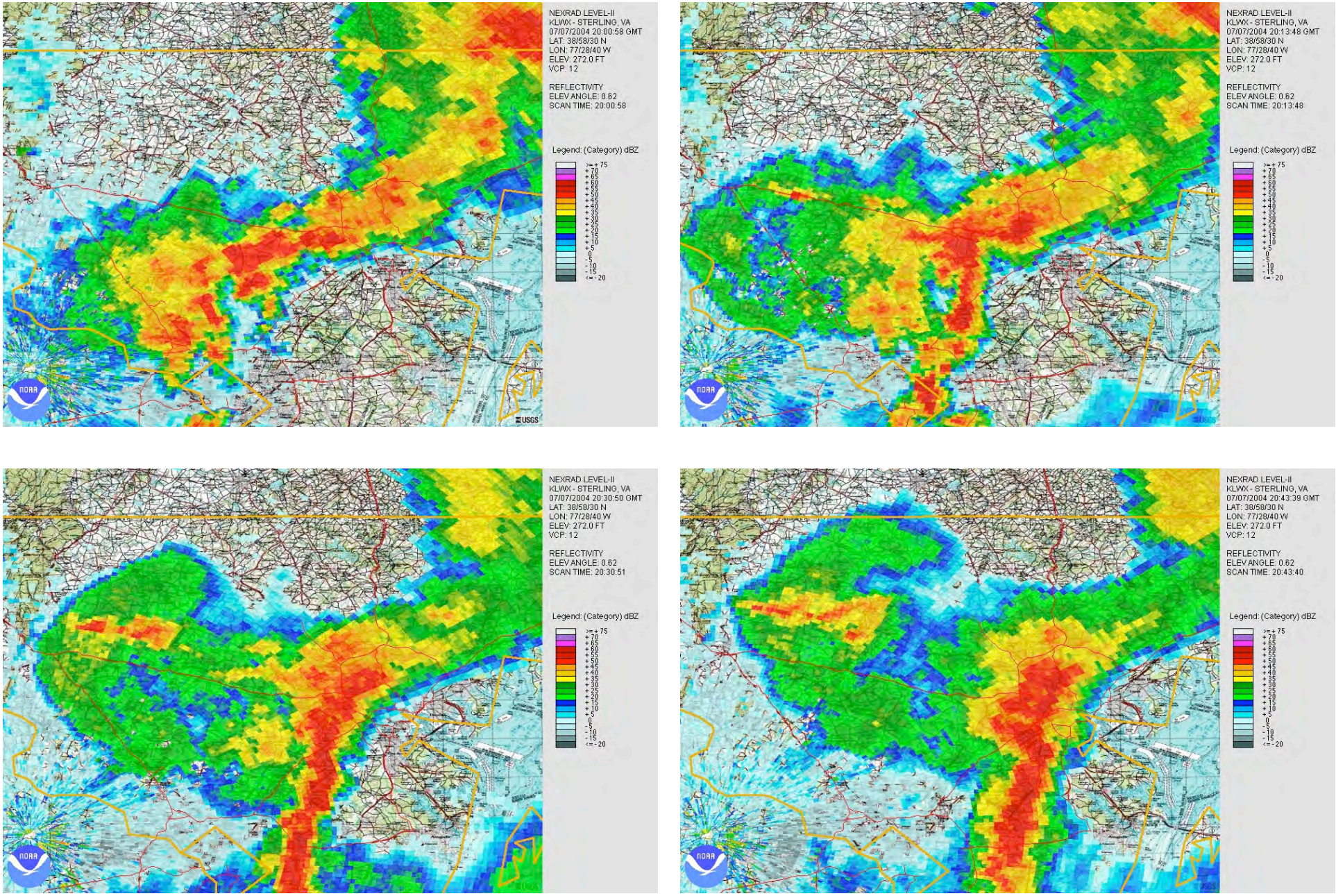

Fig. 13. Reflectivity images from the KLWX WSR-88D at: a) 2000 UTC (top left), b) 2015 UTC (top right), c) 2030 UTC (bottom left) and d) 2045 UTC (bottom right) on 7 July 2004.

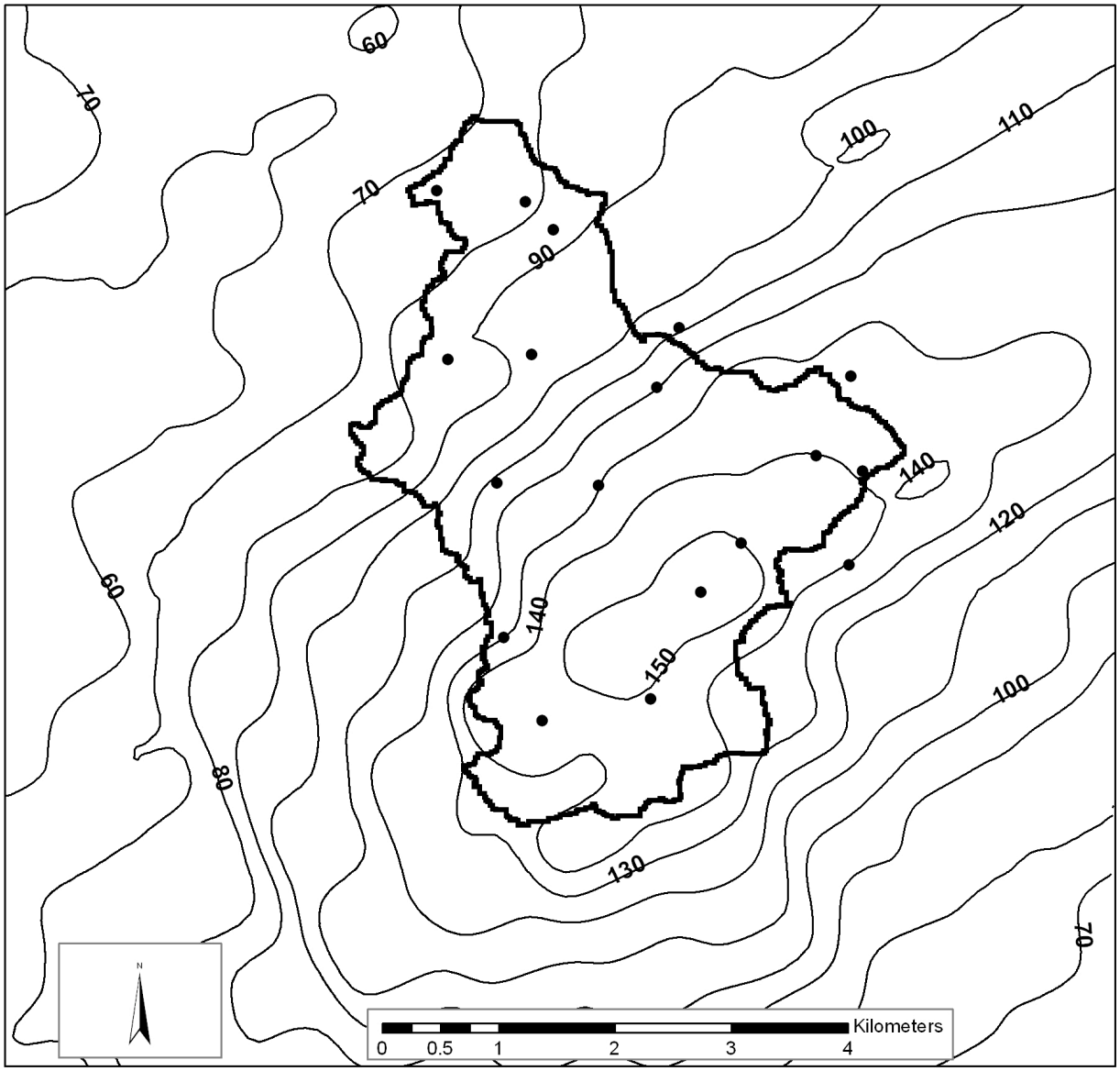

Fig. 14. Storm total rainfall map from WSR-88D rainfall analyses for the 7 July 2004 storm (with a bias correction of 1.51).

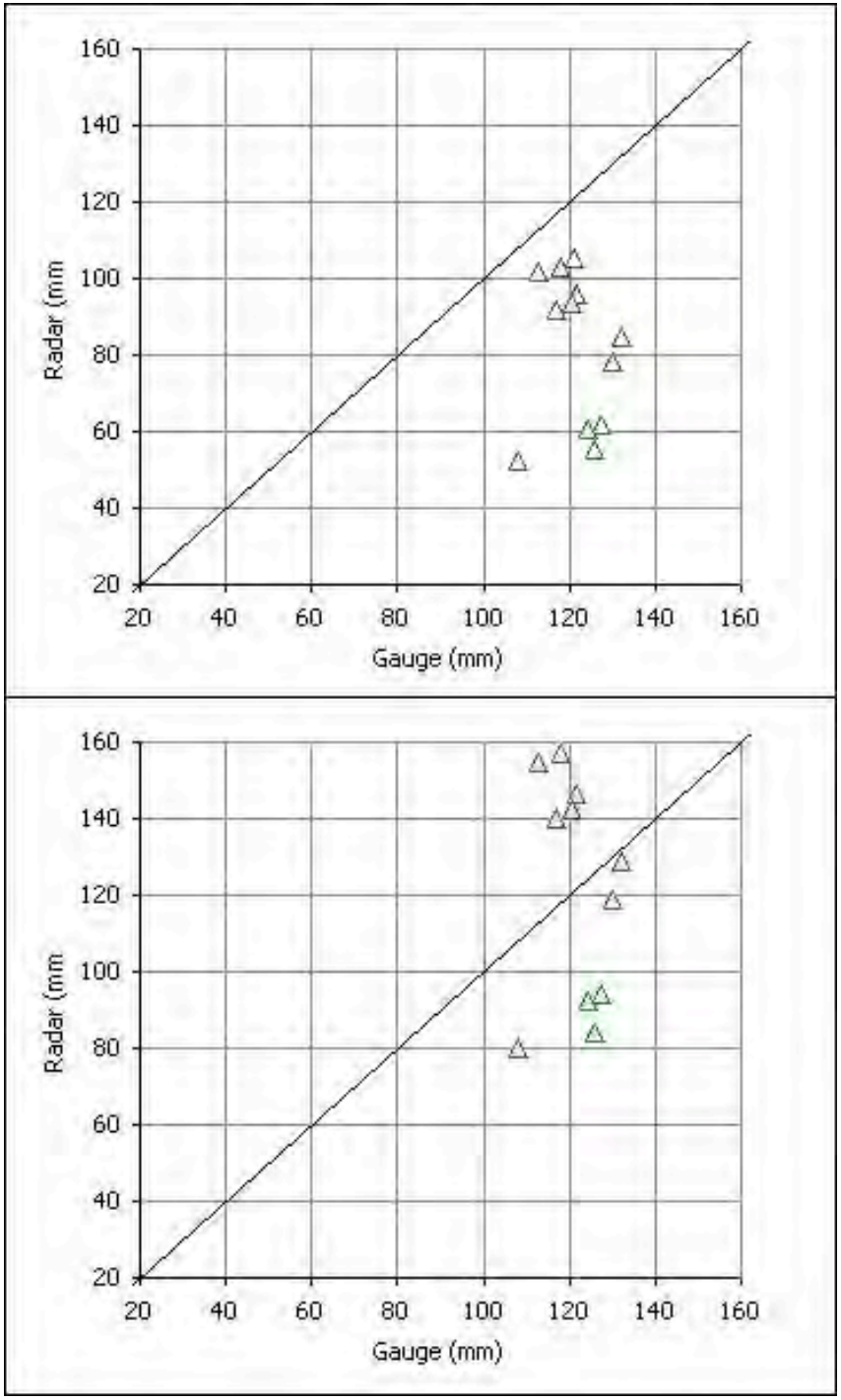

Fig. 15. Gage - radar scatterplots for the 7 July 2004 storm, without bias correction (top) and with bias correction (bottom).

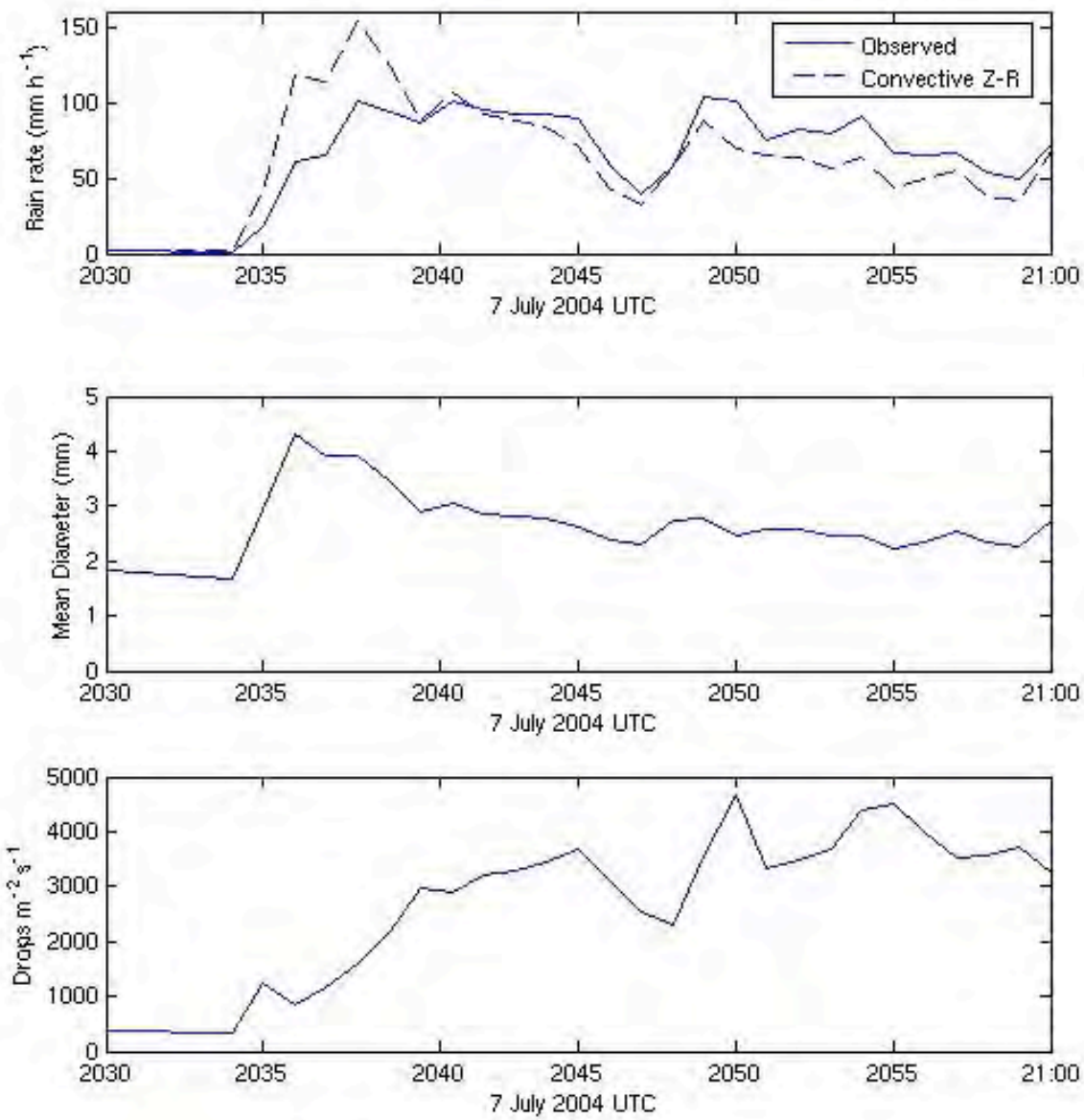

Fig. 16. Time series of: a) rainfall rate derived from disdrometer reflectivity using standard Z-R relationship (denoted by "x") and rainfall rate computed directly from disdrometer observations for the most intense period of the 7 July 2004 storm, b) mean diameter of the drop-size distribution and c) drop arrival rate of the drop-size distribution.

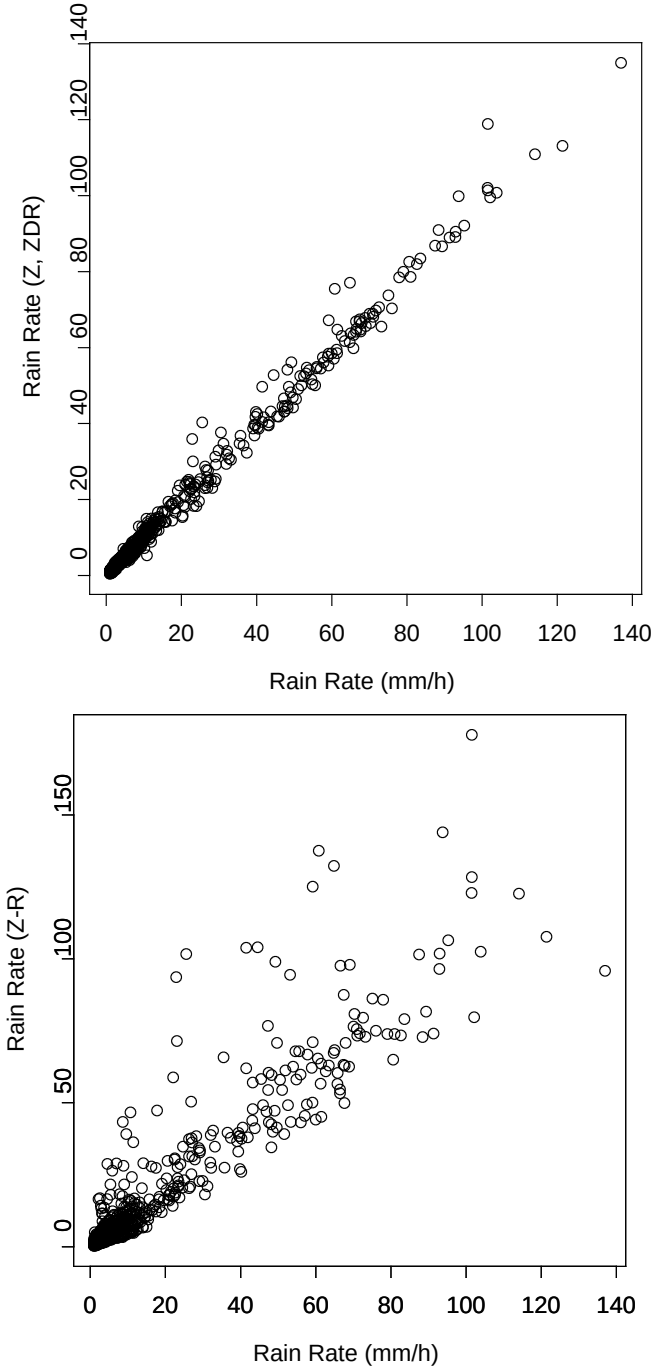

Fig. 17 Scatterplot of: a) rainfall rate computed from disdrometer measurements and rainfall rate estimated from reflectivity and differential reflectivity (computed from the disdromter observations) using the Brandes (Z, Z_{DR}) algorithm for the 7 July 2004 storm (top) and b) rainfall rate computed from Joss-Waldvogel disdrometer measurements and rainfall rate estimated from reflectivity (computed from the disdromter observations) using the convective Z-R relationship for the 7 July 2004 storm.

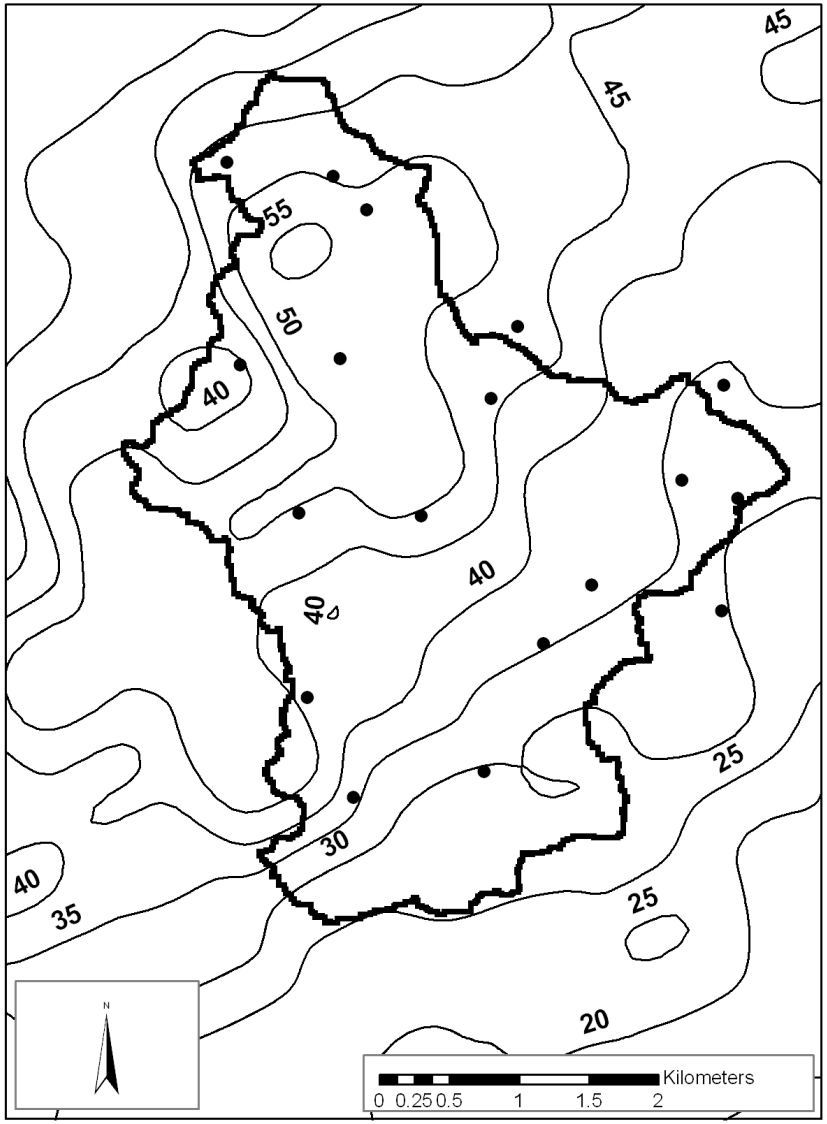

Fig. 18. Storm total rainfall (mm) for the 28 June 2005 storm.

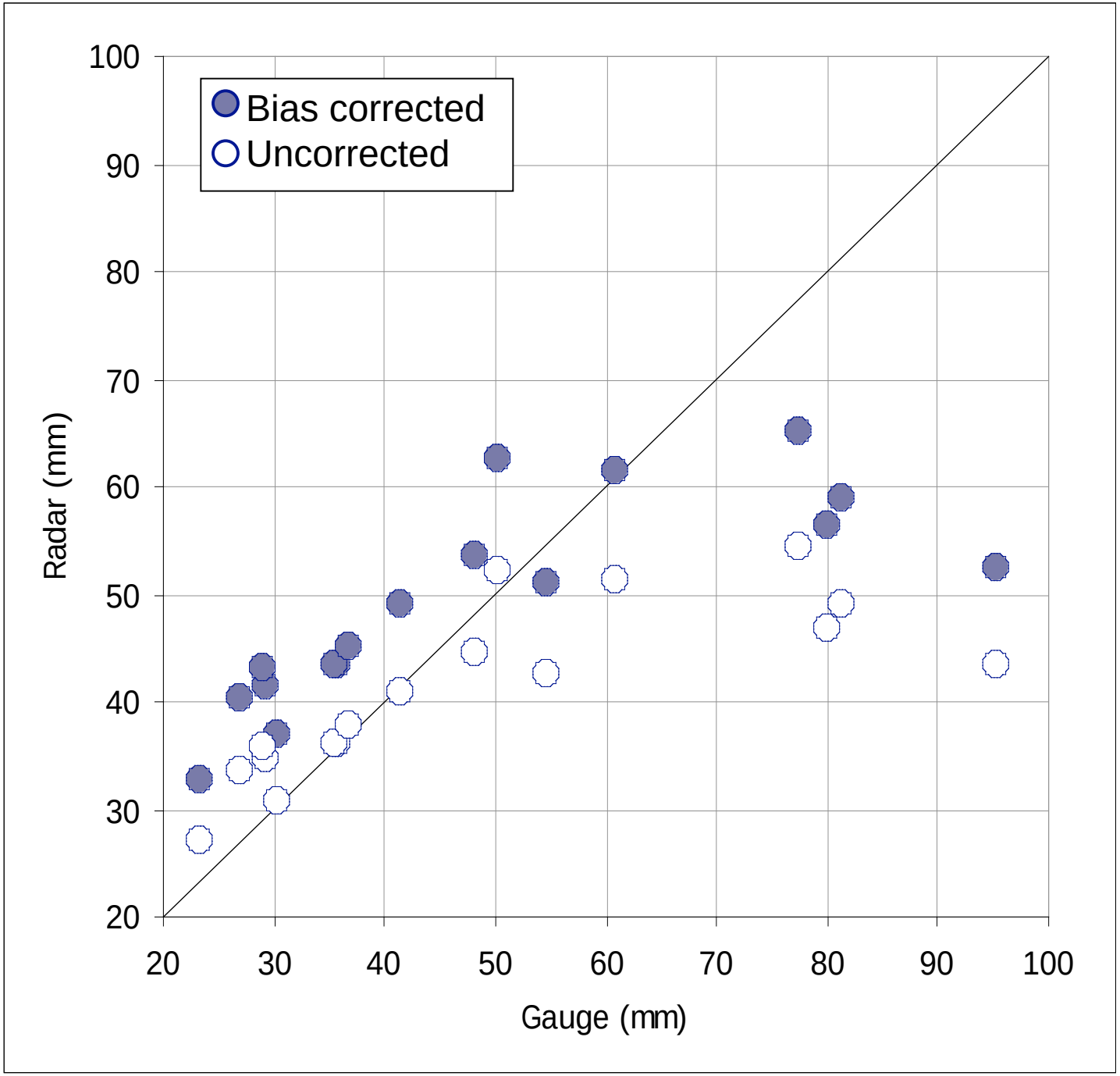

Fig. 19. Gage - radar scatterplot for the 28 June 2005 storm.

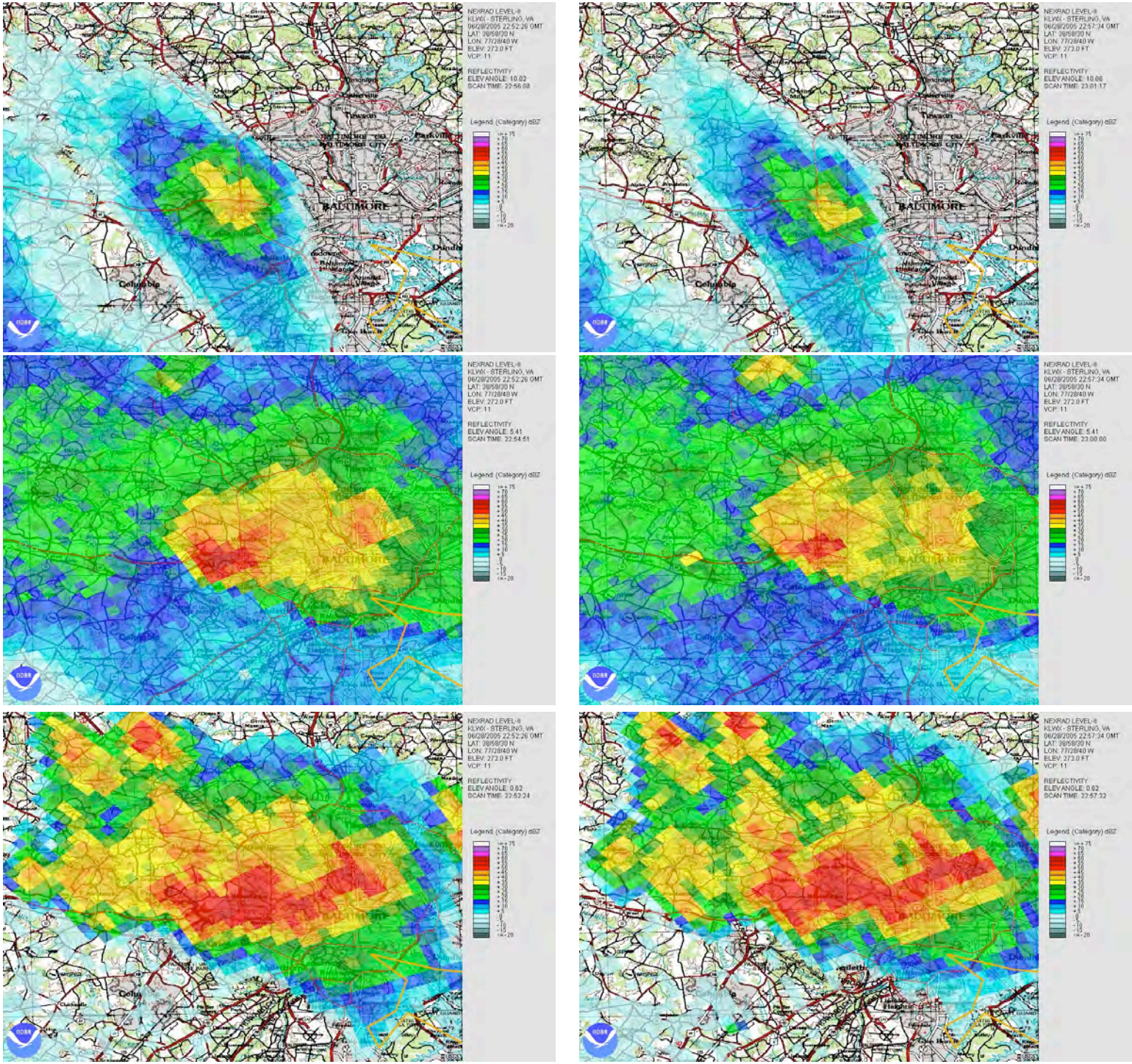

Fig. 20 KLWX reflectivity observations at 0.6 degrees (bottom), 5.0 degrees (middle) and 10 degrees (top) for the 28 June 2005 storm at: a) 2252 UTC (left) and b) 2257 UTC (right).

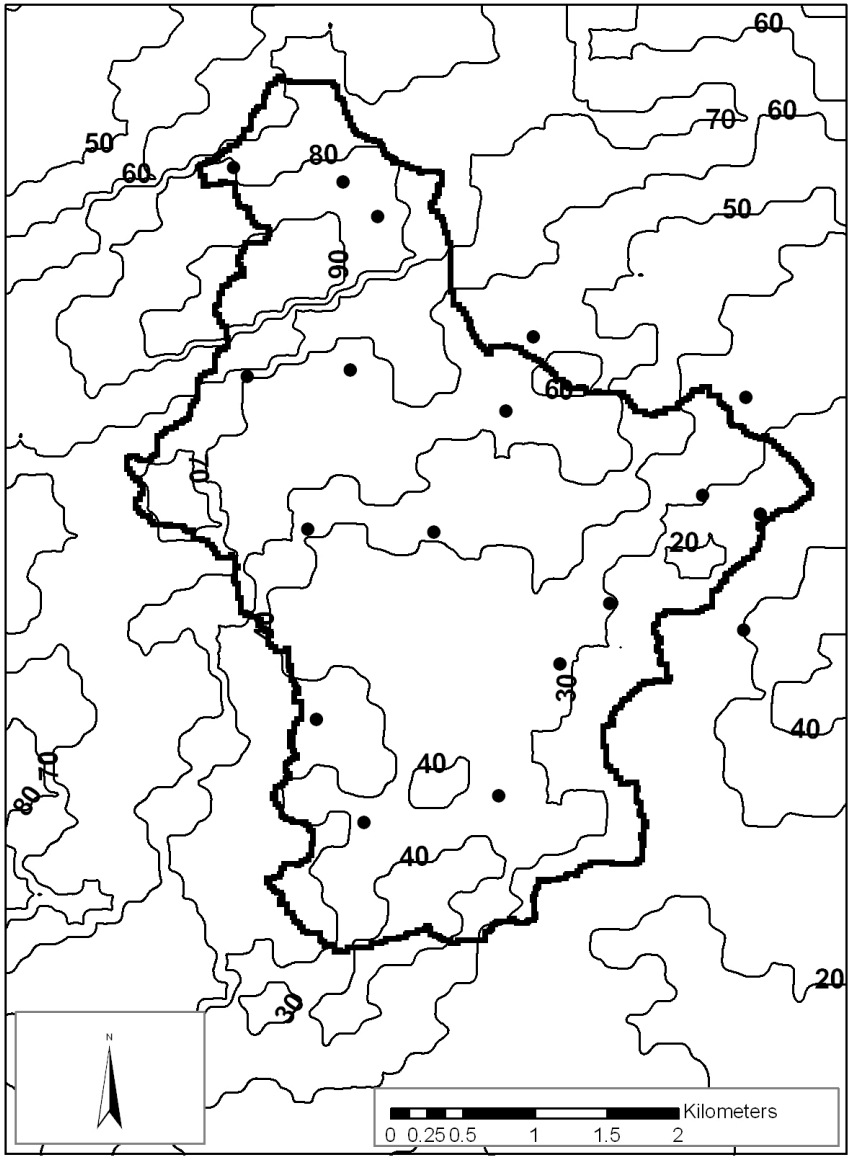

Figure 21. Storm total rainfall estimates (mm; bias-corrected) from the BWI TDWR for the 28 June 2005 storm.

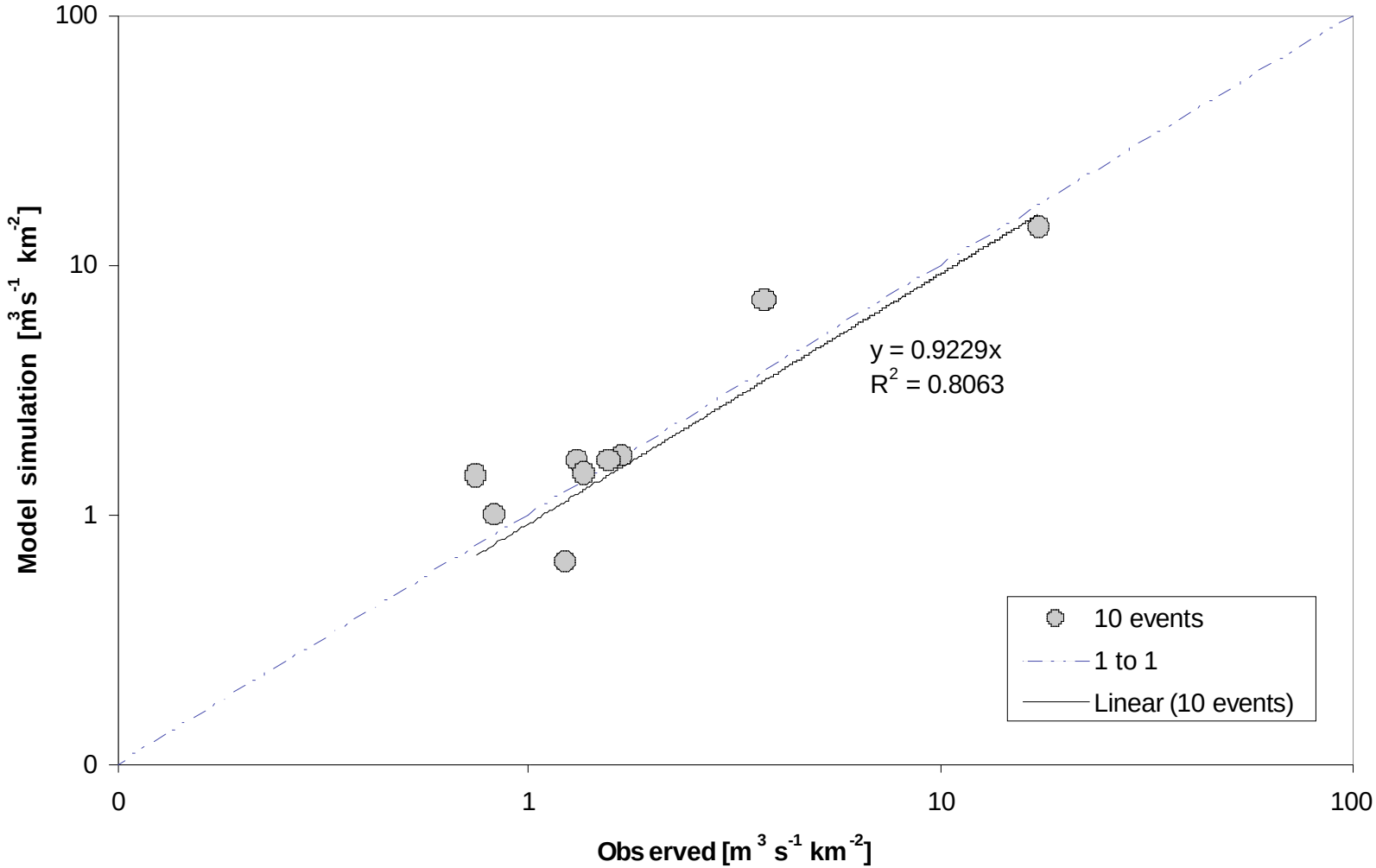

Figure 22. Comparison of the magnitude of the peak (expressed as a unit discharge) between the observed and model discharge of the ten events. Model parameters are v_0 = 0.088 m s^{-1}, v_1 = 1.7 m s^{-1}, K_S = 10 mm hr^{-1} and θ = 0.25

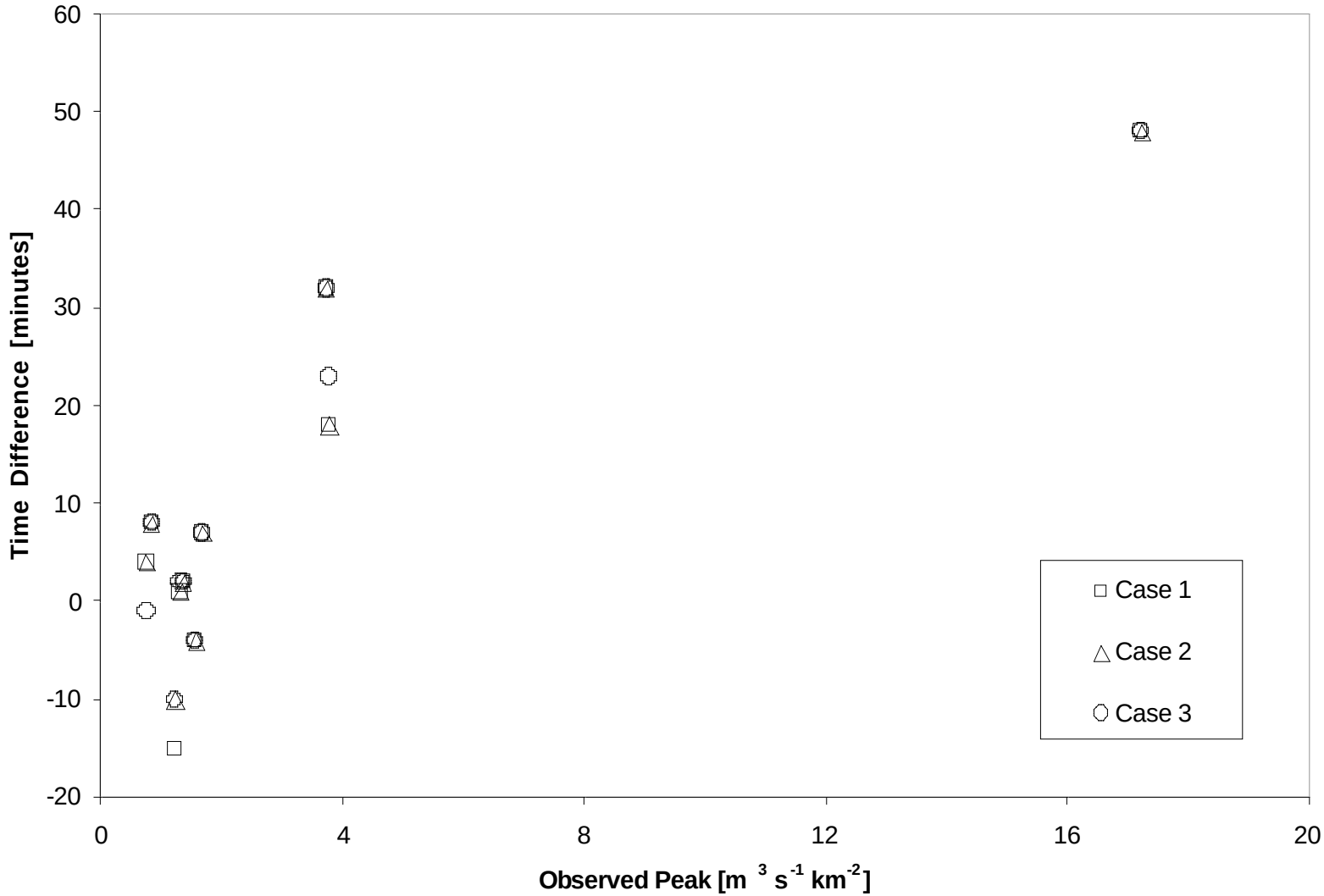

Figure 23. Difference in peak timing between observed and model discharge (expressed as a unit discharge). Negative (positive) difference indicates that the model is peaking later (earlier) than the observed. Velocity parameters for all cases are v_0 = 0.088 m s^{-1} and v_1 = 1.7 m s^{-1}. Rainfall fields for Cases 1 and 2 have bias corrections. Case 1: constant K_S, varying θ; Case 2: constant K_S constant θ with bias correction; Case 3: constant K_S, constant θ (no bias correction).

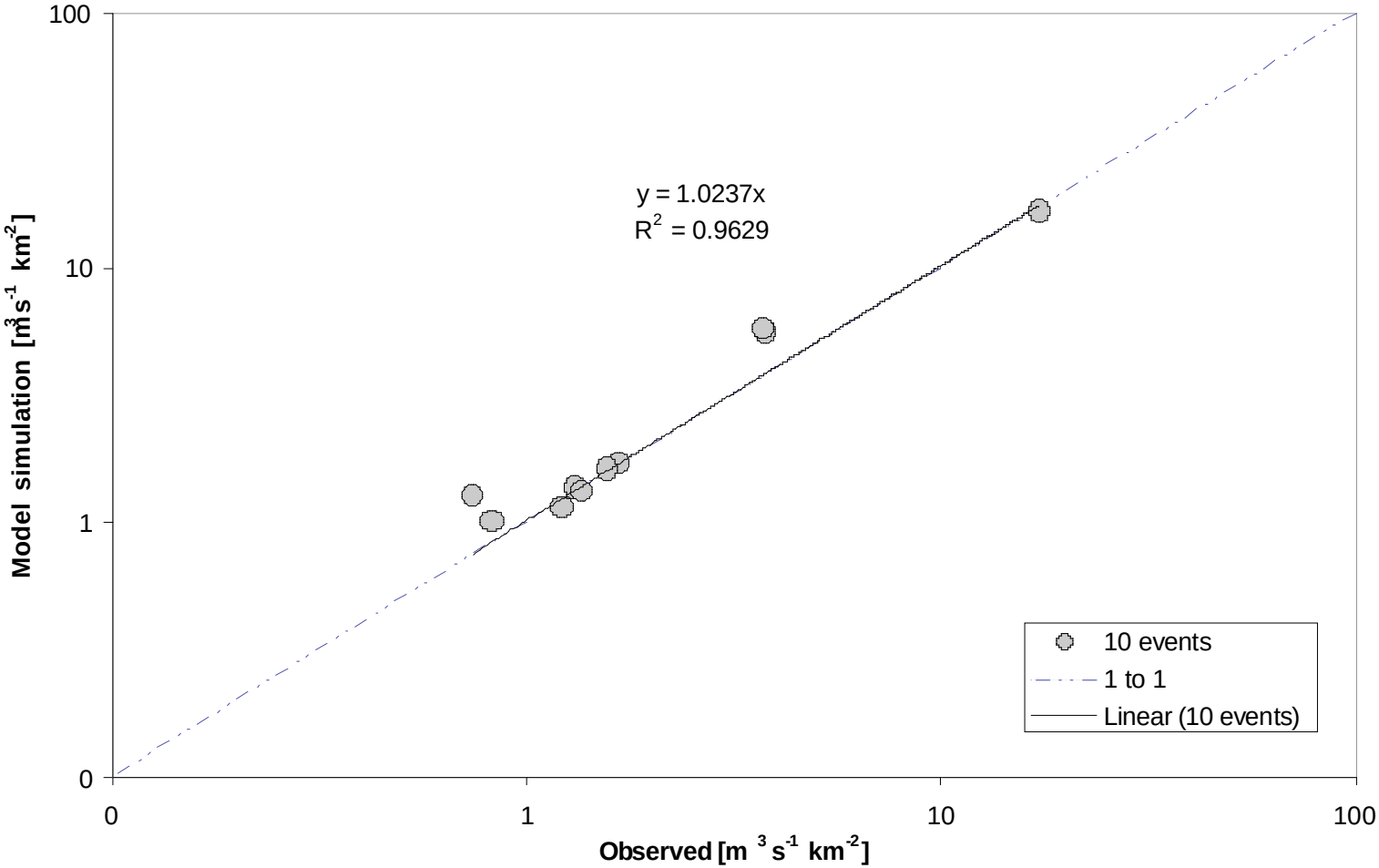

Figure 24. Comparison of the magnitude of the peak between the observed and model discharge of the ten events. Model parameters are v_0 = 0.088 m s^{-1}, v_1 = 1.7 m s^{-1}, K_S = 10 mm hr^{-1} with varying θ values.

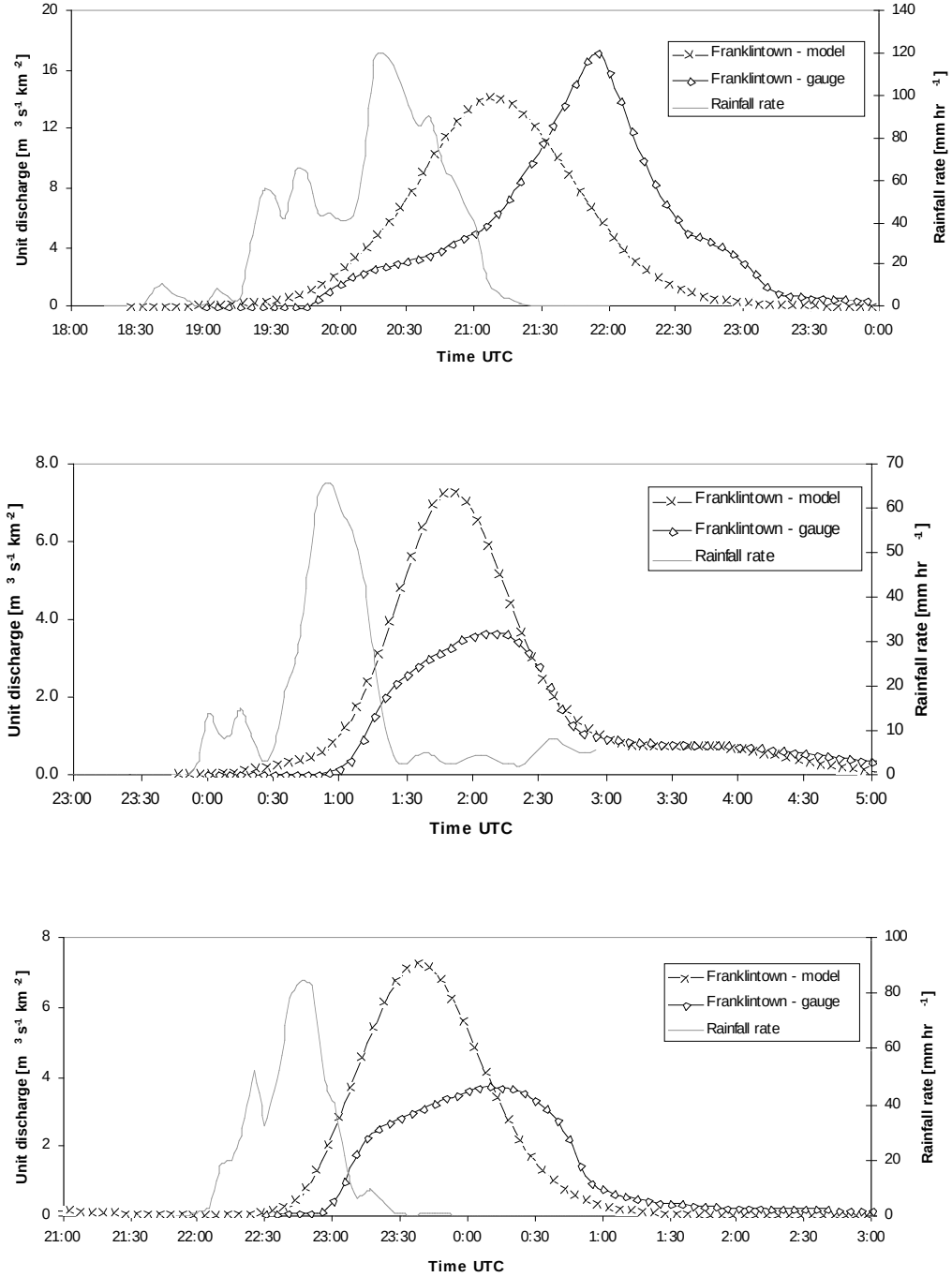

Figure 25. Comparison between observed and modeled discharge at Franklintown showing flow attenuation for: 7 July 2004 (top); 27 July 2004 (middle) and 28 June 2005 (bottom) with v_0 = 0.088 m s^{-1}, v_1 = 1.7 m s^{-1}, K_S = 10 mm hr^{-1}, θ = 0.25.

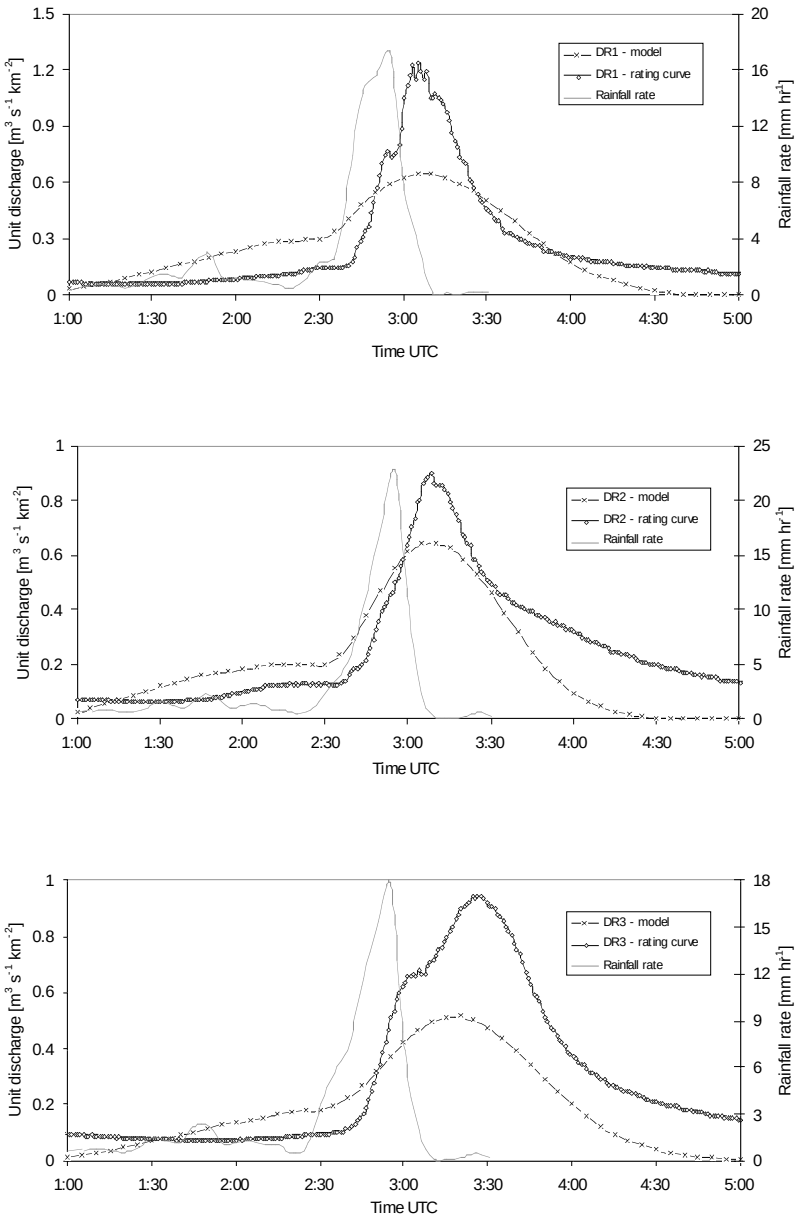

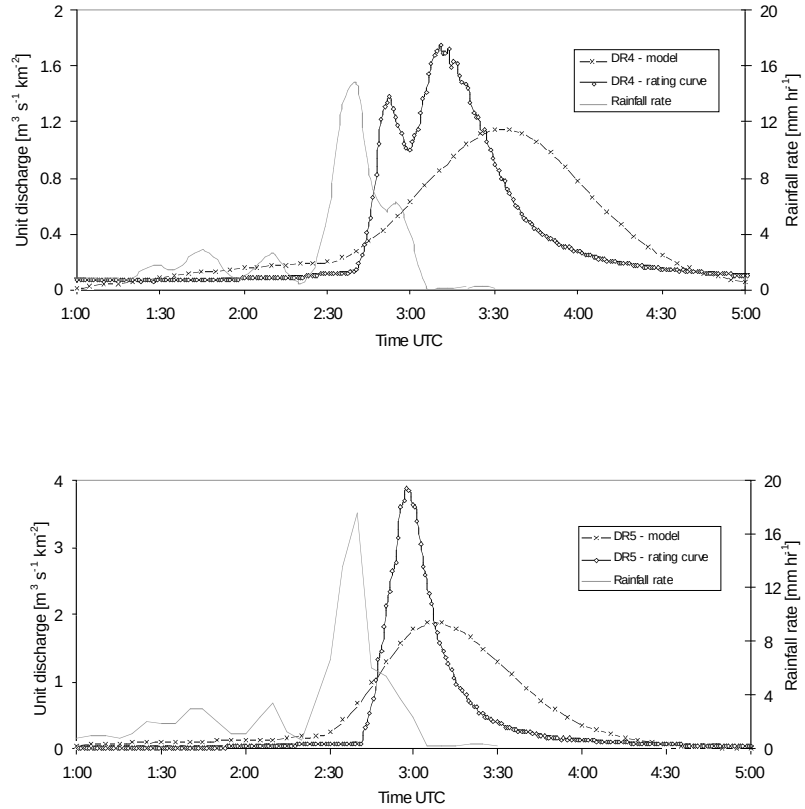

Figure 26. Model simulations for the five internal gauges for the 13 August 2004 event with parameters v_0 = 0.088 m s^{-1}, v_1 = 1.7 m s^{-1}, K_S = 10 mm hr^{-1}, and θ = 0.25.

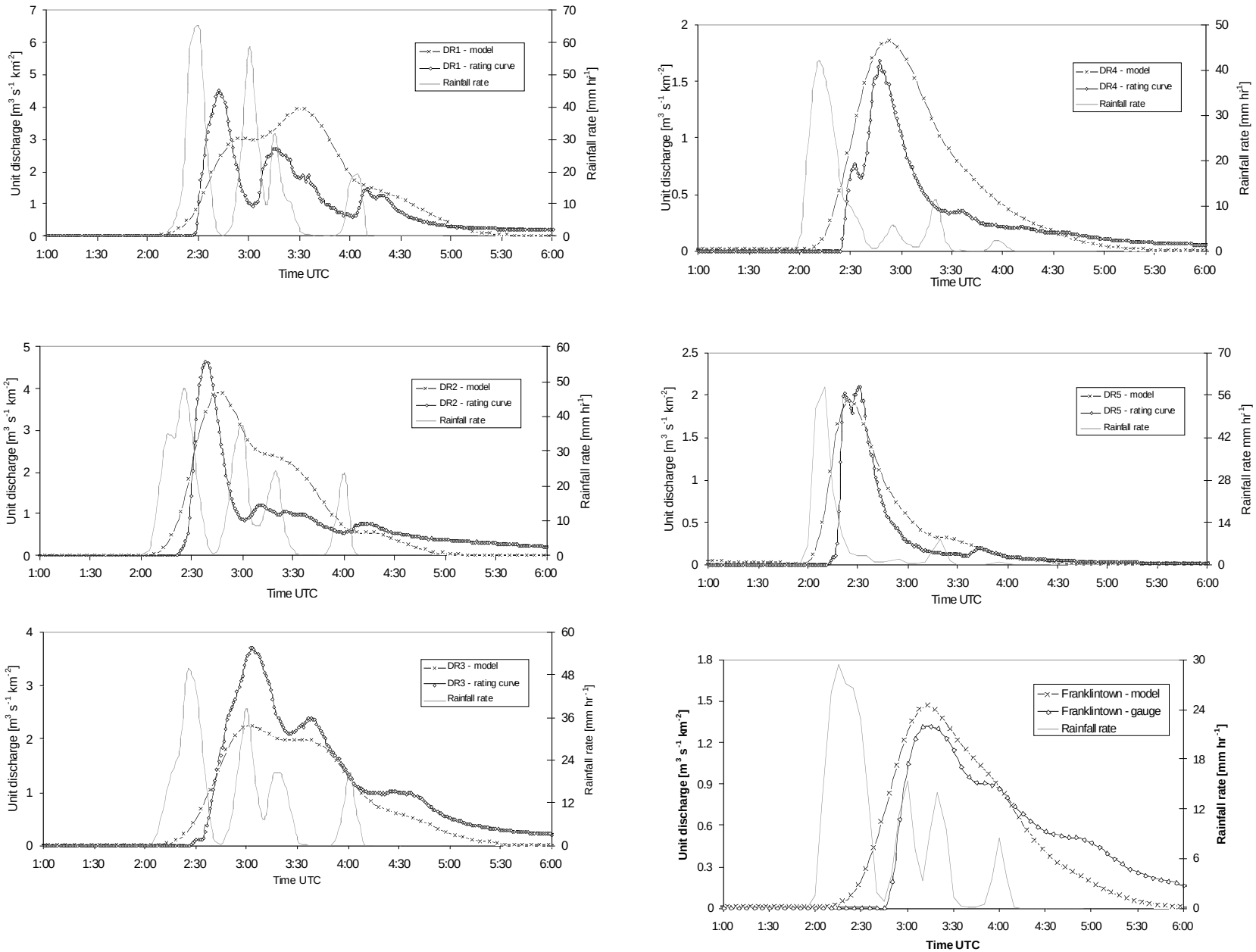

Figure 27. Model simulations for the five internal gauges for the 13 August 2004 event with parameters v_0 = 0.088 m s^{-1}, v_1 = 1.7 m s^{-1}, K_S = 10 mm hr^{-1}, and θ = 0.25.

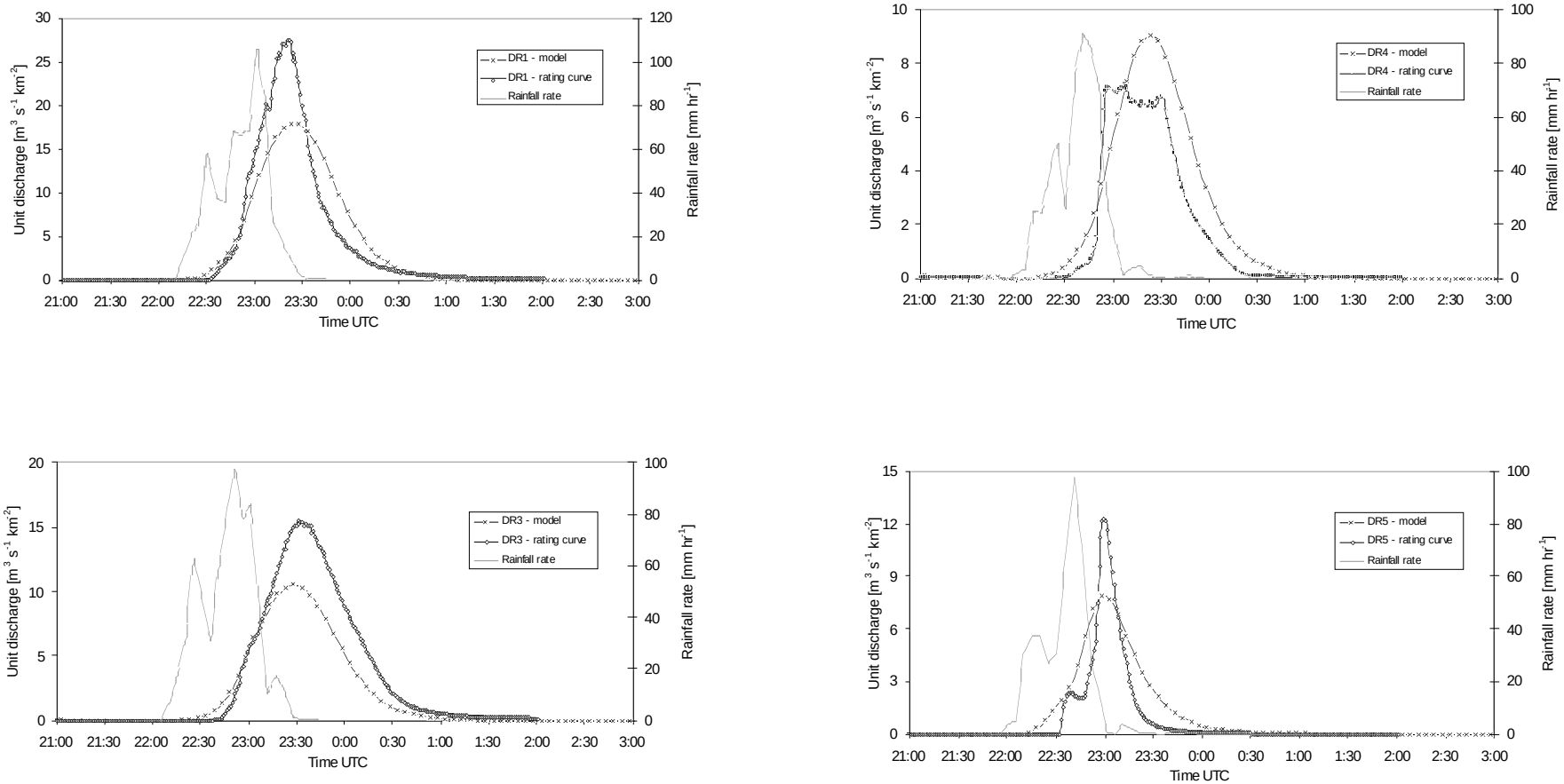

Figure 28. Model simulations for the five internal gauges for the 28 June 2005 event with parameters v_0 = 0.088 m s^{-1}, v_1 = 1.7 m s^{-1}, K_S = 10 mm hr^{-1}, and θ = 0.25.

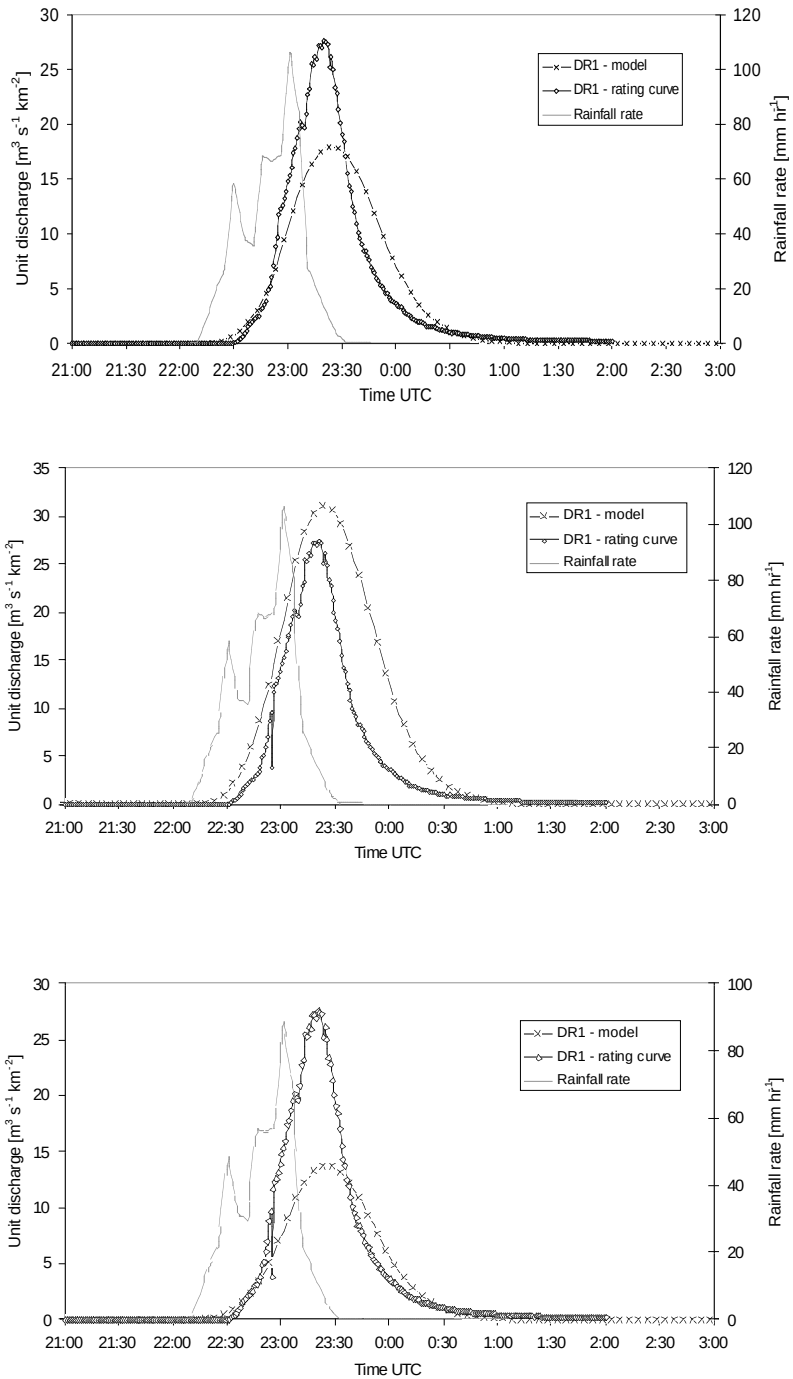

Figure 29. DR1 plots for 28 June 2005 showing model simulations when rainfall is a) bias-corrected using all available rain gauges; b) bias-corrected using gauges located only within the DR1 area; and c) not bias-corrected. Model parameters are v_0 = 0.088 m s^{-1}, v_1 = 1.7 m s^{-1}, K_S = 10 mm hr^{-1}, and θ = 0.25.

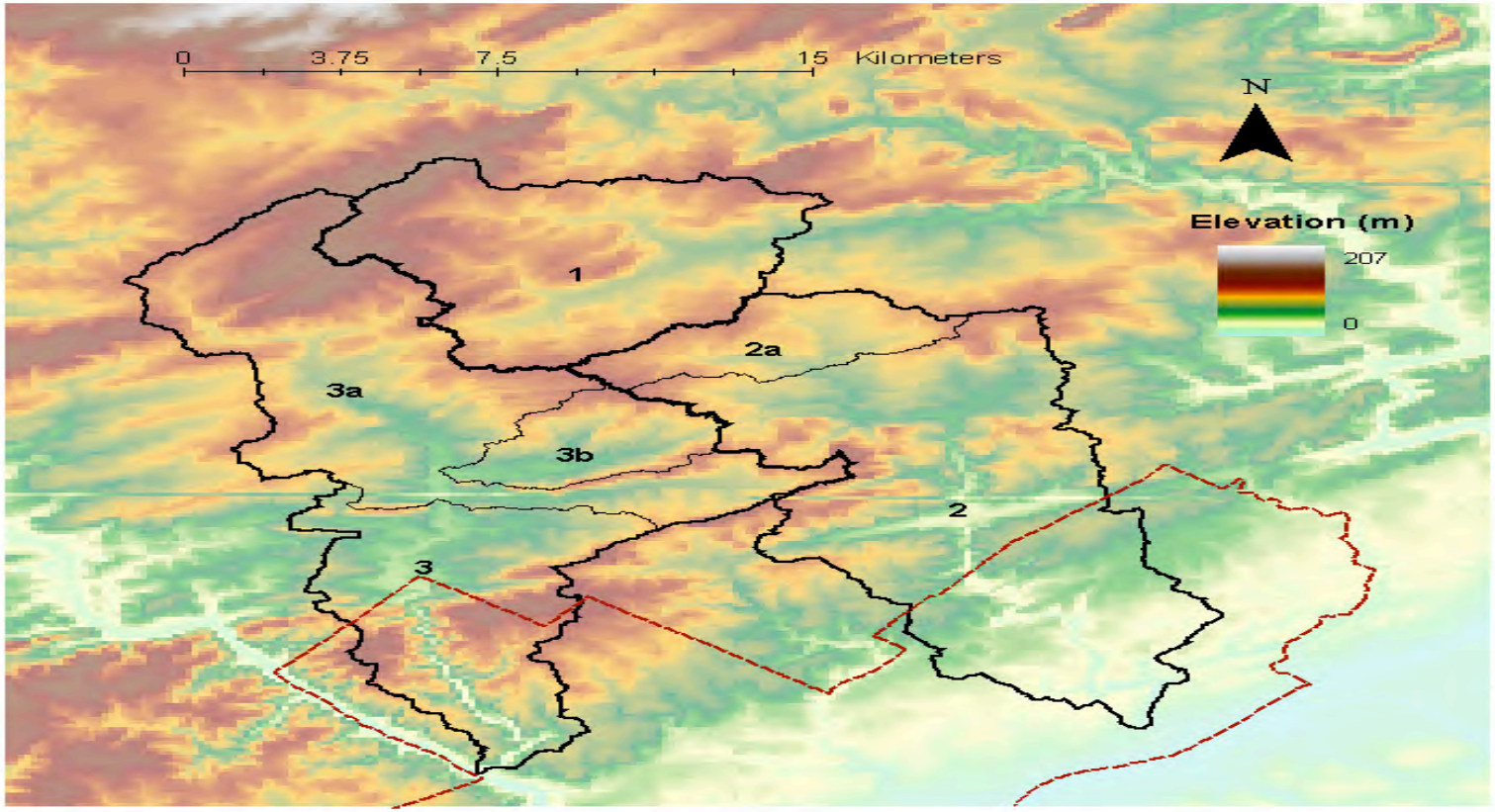

Fig. 30. Basin boundaries overlaid on a Digital Elevation Model. 1 Little Neshaminy; 2 Lower Pennypack; 2a Upper Pennypack; 3 Lower Wissahickon; 3a Upper Wissahickon; 3b Sandy Run. Philadelphia is outlined in red.

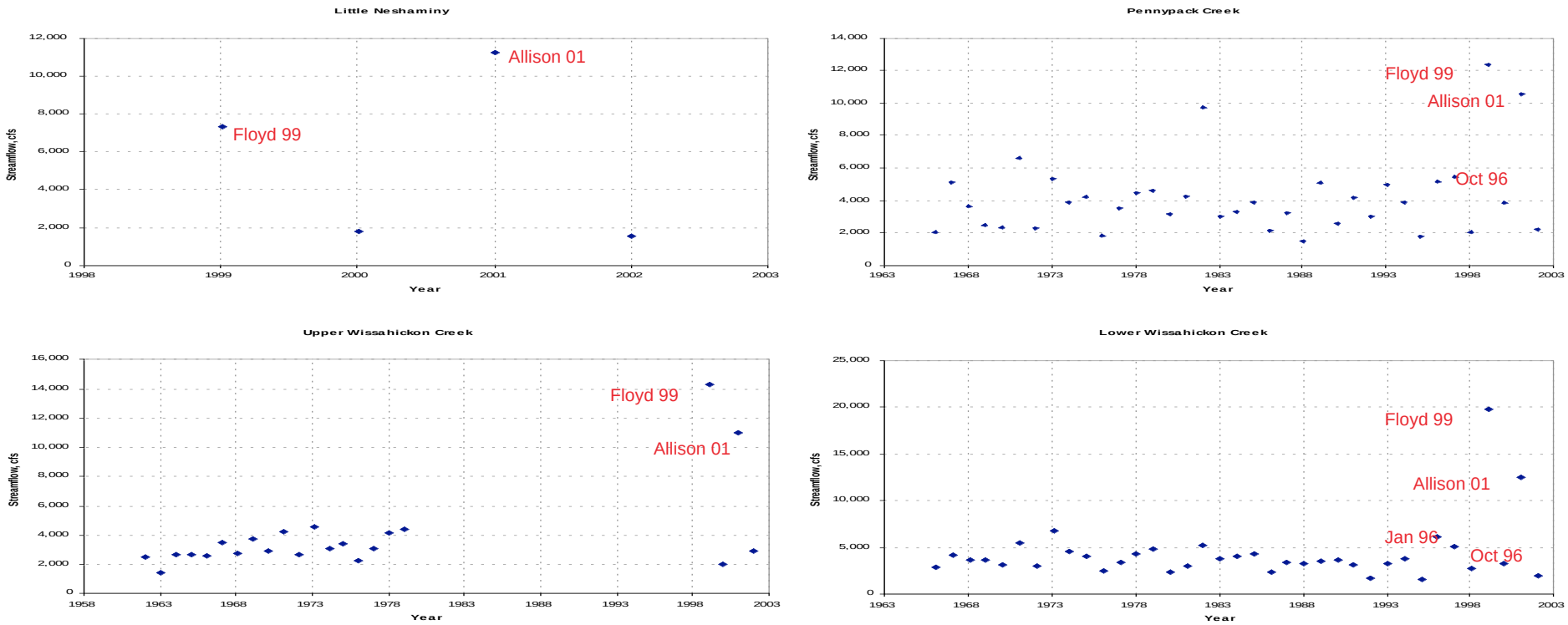

Figure 31. USGS annual peak streamflow for Little Neshaminy (upper left), Pennyack Creek (upper right), upper Wissahickon (lower left) and lower Wissahickon (lower right), showing magnitude of September 1999 (Floyd), June 2001 (Allison), January 1996 and October 1996 flood peaks (see Fig 30 for basin locations).

Convective Z-R

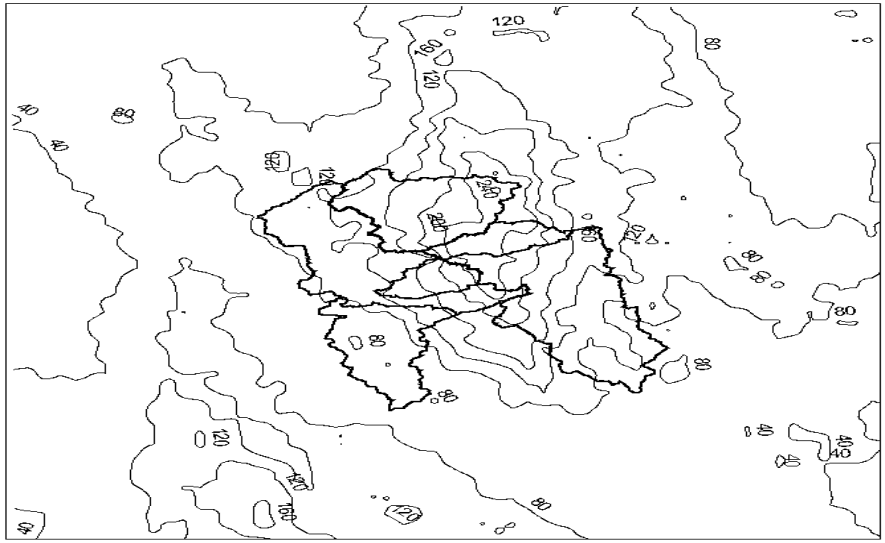

Tropical Z-R

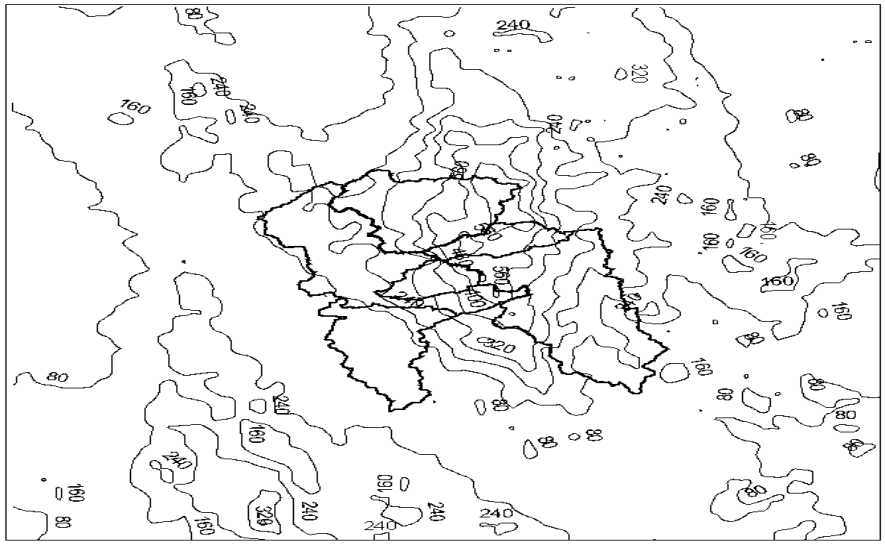

Figure 32. Comparison of storm total accumulation (mm) for TS Allison between convective Z-R (top) and tropical Z-R (bottom).

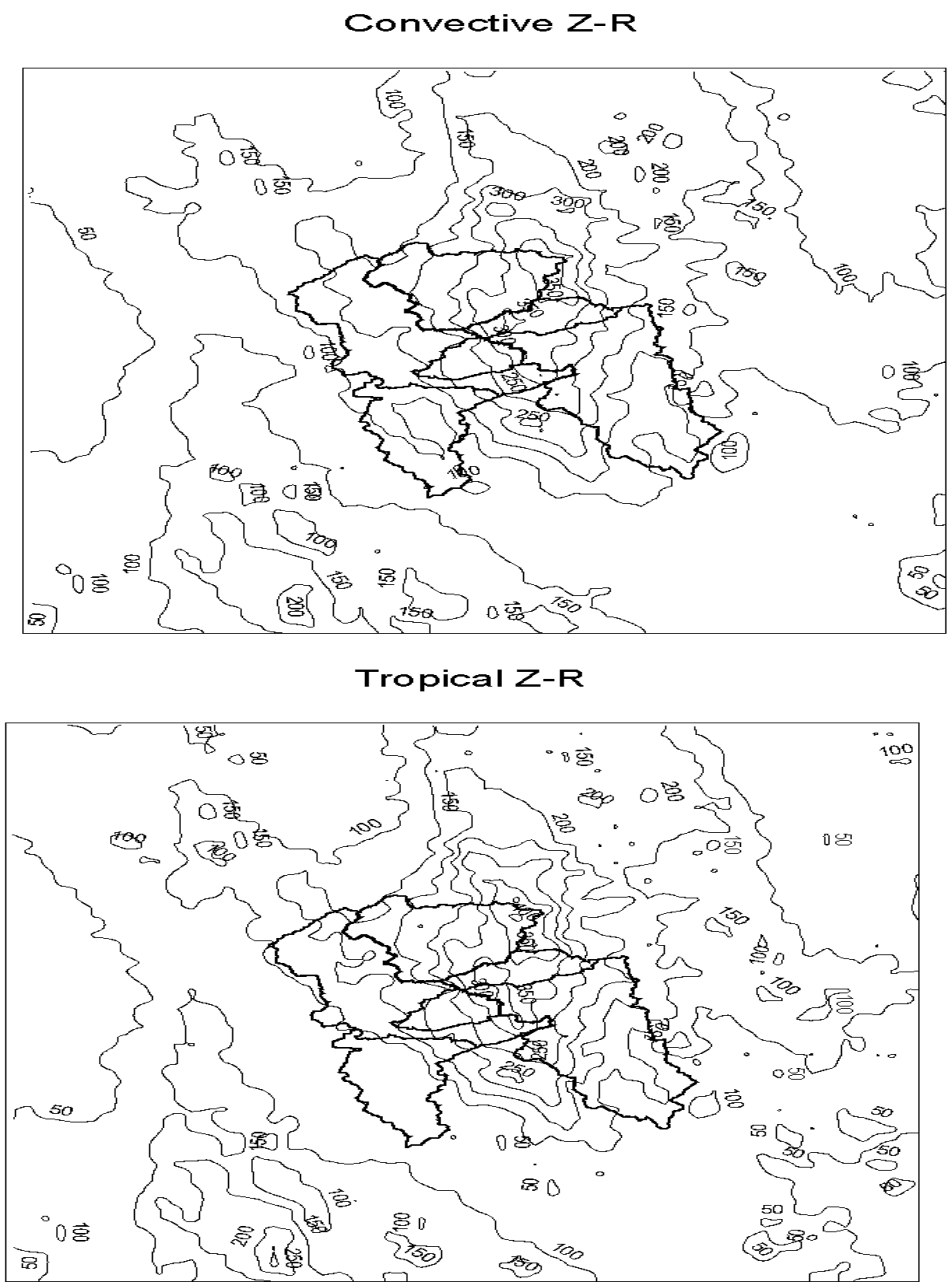

Figure 33. Comparison of storm total accumulation (mm) for TS Allison between bias-corrected convective Z-R (top) and bias-corrected tropical Z-R (bottom).

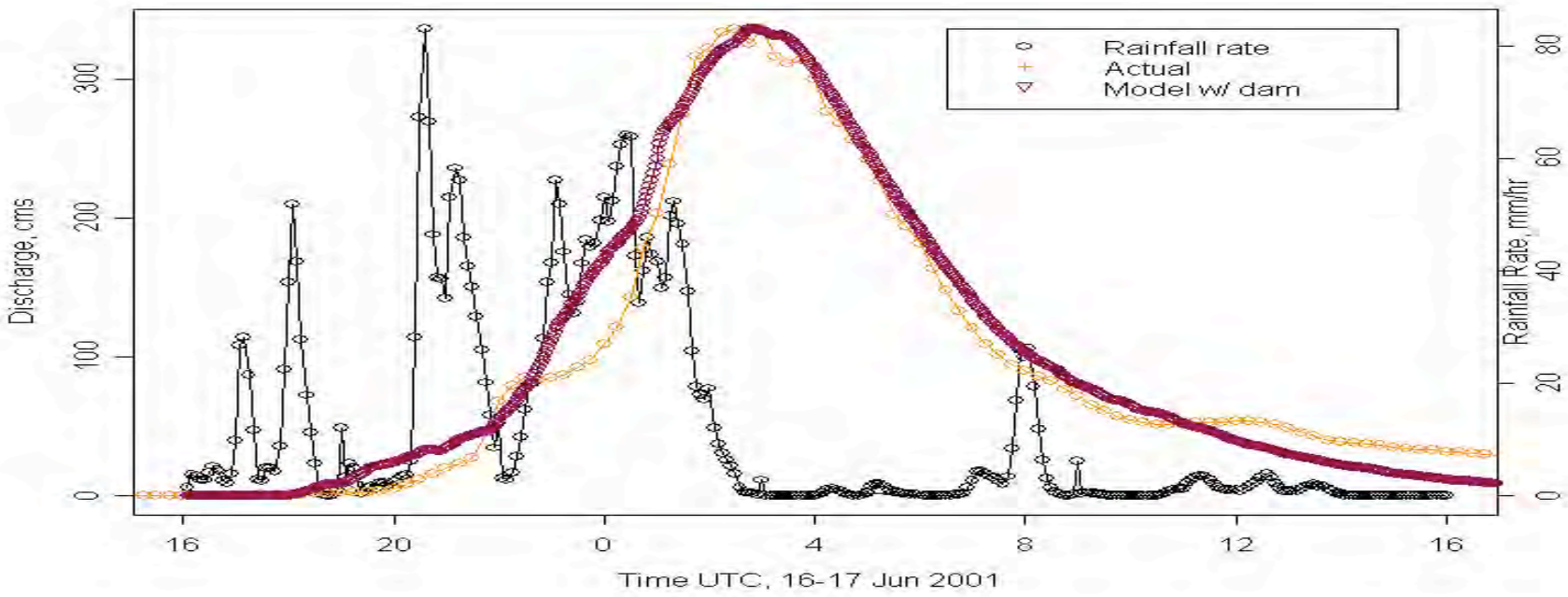

Figure 34. Basin-averaged rainfall rate, observed discharge and discharge simulated by the Network Model for the 16-17 June 2001 flood in Little Neshaminy Creek.

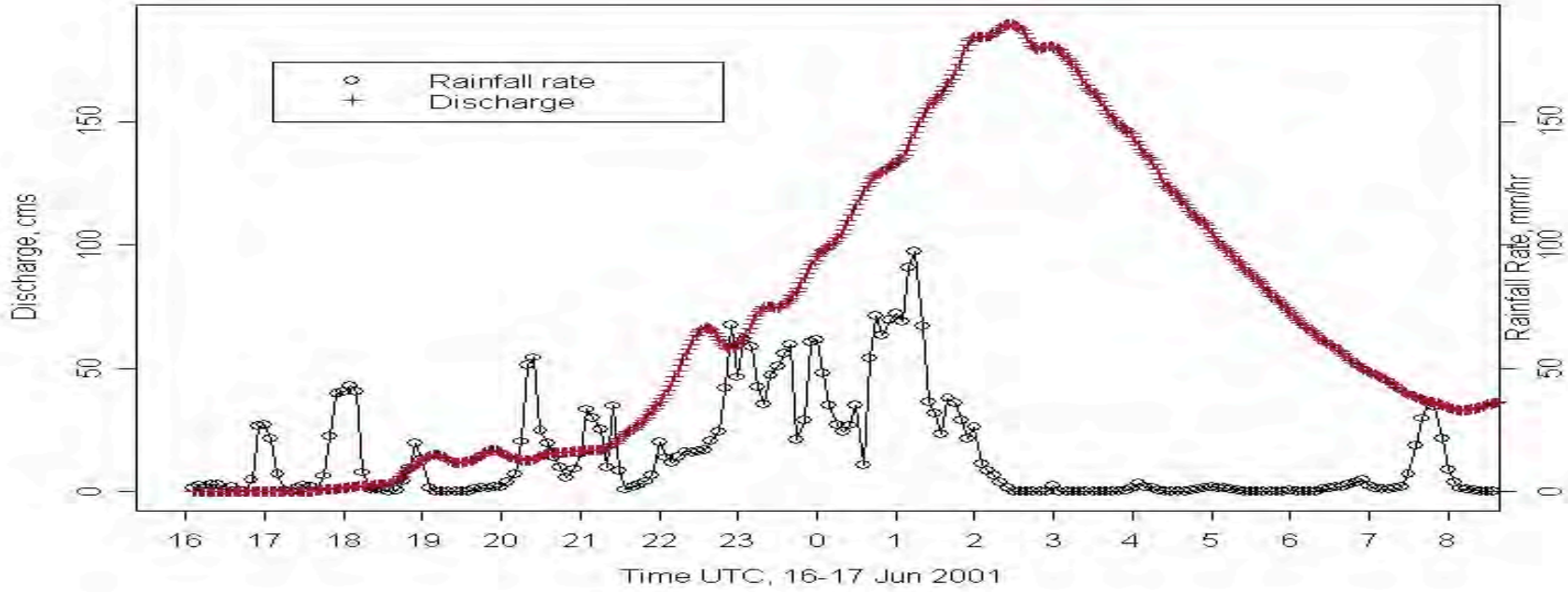

Figure 35. Basin-averaged rainfall rate and discharge simulated by the Network Model for the 16-17 June 2001 flood in upper Pennypack Creek (drainage area of 20 km^2).